
Article:
Soltanahmadi, S, Murray, BS orcid.org/0000-0002-6493-1547 and Sarkar, A orcid.org/0000-0003-1742-2122 (2022) Comparison of oral tribological performance of proteinaceous microgel systems with protein-polysaccharide combinations. Food Hydrocolloids. ISSN 0268-005X

https://doi.org/10.1016/j.foodhyd.2022.107660

Comparison of oral tribological performance of proteinaceous microgel systems with protein-polysaccharide combinations

Siavash Soltanahmadi, Brent S. Murray, Anwesha Sarkar*

Food Colloids and Bioprocessing Group, School of Food Science and Nutrition, University of Leeds, UK

*Corresponding author:

Prof. Anwesha Sarkar

Food Colloids and Processing Group,

School of Food Science and Nutrition, University of Leeds, Leeds LS2 9JT, UK.

E-mail address: A.Sarkar@leeds.ac.uk (A. Sarkar).

19 **Graphical Abstract**

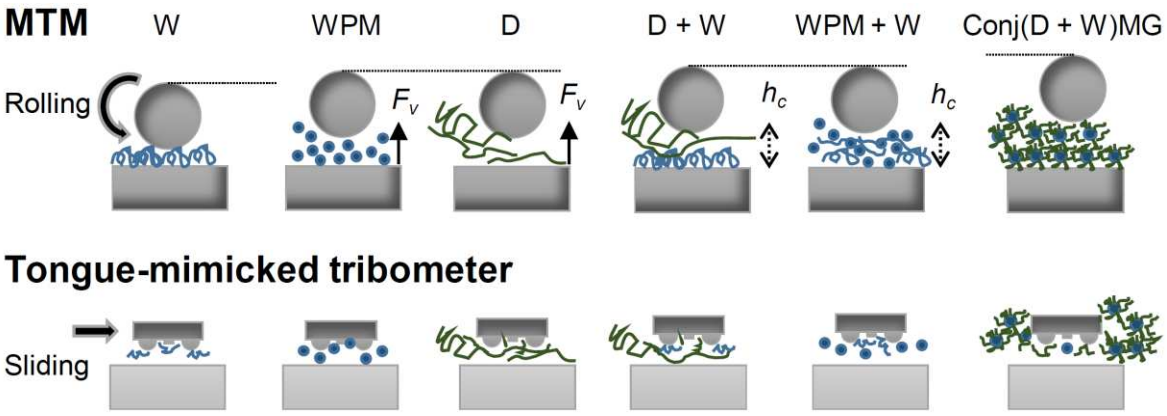

20

21

Highlights

- Whey protein microgels (WPM) provide fluid-film and boundary lubricity
- WPM (41.7 vol%) deliver the same thickening behaviour as dextran (D) at 5 wt%
- WPM can be used as replacer for thickeners and lubrication-enhancer, simultaneously
- Microgels of D-conjugated whey protein deliver superlubricity upon entrained
- Superlubricity of conjugated microgels disappeared in a tongue-mimicked tribometer

Abstract

Polysaccharides are often used as rheology modifiers in multiphasic protein-rich food systems. Recently, proteinaceous microgels have garnered research attention as promising lubricating agents. However, whether proteinaceous microgels can be used to replace polysaccharides in a tribological context remains poorly understood. In this study we compared the flow and oral-tribological behaviour of Newtonian solutions of the polysaccharide dextran (D, 1-11 wt%) when combined with a dispersion of whey protein isolate (W, 1-13 wt%) or whey protein microgel (WPM, 41.7 vol%) and compared with microgels of D-conjugated to W (Conj(D[11] + W[5])MG) or dispersions of WPM in W solutions. W and WPM alleviated frictional forces between elastomeric surfaces as well as biomimetic tongue-like surfaces in the boundary lubrication regime. Despite the negligible influence of D on the thin-film lubricity, its impact on viscous-facilitated lubricity was significant. The importance of measurements with the tongue-mimicked setup emerged where Conj(D[11] + W[5])MG did not show significant lubricity enhancement despite its outstanding performance with conventional tribo-testing setups. By optimising a combination of WPM and non-microgelled W, we demonstrate that a combined viscous and thin-film lubricity could be achieved through a single-protein-component without the need of polysaccharides. The dispersions of WPM (41.7 vol%) deliver the same flow and viscous-friction behaviour to that of 5 wt% D and excel in thin-film lubricity. These findings pave the way towards design of processed foods with clean labels, taking advantage of using a single proteinaceous moiety whilst delivering enhanced lubricity and viscosity modification without the need of any additional thickener.

Keywords: Oral tribology; Tongue-mimicked; Microgel; Polysaccharide, Protein-Polysaccharide; Viscosity; Lubrication; Conjugate

1. Introduction

Polysaccharides are widely used in the food industry, thanks to their non-toxic properties, accessibility and sustainability characteristics whilst imparting remarkable rheological properties that provide well-recognised favourable textural attributes (Yang, Li, Li, Sun, & Guo, 2020). Dextran (D) is a biocompatible, hydrophilic, neutral and branched food polysaccharide sourced from metabolites secreted from micro-organisms (Yang, 2020), and mainly composed of α(1→6) linkage with side chain branching (α (1→3)) attached to the backbone glucose units (Perrino, Lee, & Spencer, 2009). D also has broad applications in pharmaceutical products (e.g. as drug delivery vehicles) (Perrino, Lee, Choi, Maruyama, & Spencer, 2008) and has been subjected to tribological examinations when grafted onto surfaces as brushes, to mediate lubricity (Goren, Spencer, & Crockett, 2014; Perrino, 2008; Perrino, 2009; Rosenberg, Goren, Crockett, & Spencer, 2011).

Food proteins are extensively used to generate complex colloidal food systems possessing improved nutritional and structural functionality, including thickening and stabilization of emulsions (Araiza-Calahorra, Glover, Akhtar, & Sarkar, 2020; Sarkar, et al., 2016). Whey protein isolate (W), a food globular protein mainly composed of *β*-lactoglobulin (*β*-lg), *α*-lactalbumin (*α*-la) and bovine serum albumin, has been actively investigated in it's native, denatured or microgel form to enhance food product characteristics (Zembyla, et al., 2021). Microgels are particles ranging in size from a few tens of nm to a few tens of μm and consist of a fluid phase retained within a cross-linked network of macromolecules. Whey protein microgels (WPM) have shown exceptional ability as Pickering stabilizers of oil-in-water (O/W) emulsions that can also delay lipase digestion of such emulsions (Sarkar, 2016), act as fat replacers (Liu, Tian, Stieger, van der Linden, & van de Velde, 2016) and also as aqueous lubricants in

orally relevant conditions (Andablo-Reyes, et al., 2019; Sarkar, Kanti, Gulotta, Murray, & Zhang, 2017). WPM are typically formed via heat-treatment of aqueous solutions of W (typically at ≥ 65 °C), resulting in internal cross-linking of the molecules via hydrogen bonding, hydrophobic interactions and disulfide bonding, under the appropriate conditions, to form the internal microgel biopolymer network (Araiza-Calahorra, 2020; Sarkar, 2017; Sarkar, 2016). While a thin-film adsorption-based mechanism, prompting *hydration* lubrication mechanism (Klein, 2013), has been proposed to explain the lubricity of W dispersions (Sarkar, Andablo-Reyes, Bryant, Dowson, & Neville, 2019; Zembyla, 2021), the lubricity of WPM was mainly attributed to a ball-bearing (or rolling) property of the entrained WPM particles into the contact interface (Liu, 2016; Sarkar, 2017).

Among other numerous efforts to improve the functionality of proteins, covalent conjugation of polysaccharide to proteins via the Maillard reaction has gained interest since it does not require any extraneous chemicals (Araiza-Calahorra, 2020; Sun, et al., 2011; Yang, 2020). Maillard conjugation has been used to boost protein properties in food applications, including enhanced resistance when subjected to environmental stresses (pH, ionic strength etc.), and improved protein solubility, stability (heat-induced aggregation etc.) and emulsifying properties (Araiza-Calahorra, 2020; Oliver, Melton, & Stanley, 2006). Conjugation is achieved simply by thermal treatment at an appropriate pH and appropriate water activity, leading to the condensation of the reducing end of the sugar in D with a deprotonated primary amino group of W, resulting in glycosylation (Araiza-Calahorra, 2020; Sun, Yu, Yang, , 2011).

Tribology has been proven to be a prominent tool to elucidate textural perception of food systems and to shed light on the links between sensory data and instrumental data (Pradal & Stokes, 2016; Sarkar, 2017; Sarkar & Krop, 2019; Sarkar,

105 Soltanahmadi, Chen, & Stokes, 2021; Stokes, Boehm, & Baier, 2013). The mini
106 traction machine (MTM2, PCS instruments, UK), as a bench-top instrument, has been
107 extensively used to characterise the tribological performance of fluid/ semi-fluid/ solid
108 substances particularly in oral-tribology investigations by means of providing the
109 friction coefficient (μ) data. Although the MTM2 has offered substantial insights into
110 the tribology of food systems, it does not well represent the type of tribocontact
111 conditions and materials involved in real mouth conditions. Recently, a method has
112 been developed by Andablo-Reyes et al. (Andablo-Reyes, et al., 2020) which uses
113 elastomeric surfaces mixed with a surfactant (Span 80) to create dome and pillar-
114 shaped features that endow the contact surfaces with mechanical, wettability and
115 surface texture characteristics much closer to that of the real tongue: the tongue-
116 mimicked setup (Andablo-Reyes, 2020).

117 Although the tribological behaviour of suspensions of colloidal microgel
118 systems and some food polysaccharides (pectin, xanthan, gellan, carrageenan and
119 etc.) have been investigated in the literature (Andablo-Reyes, 2019; Sarkar, 2017;
120 Stokes, Macakova, Chojnicka-Paszun, de Kruif, & de Jongh, 2011), no attempt has
121 been made to understand the lubrication performance of polysaccharide-conjugated
122 W, to the best of the authors' knowledge. Further, proteinaceous compounds have
123 been suggested as fat-replacers but whether or not modified proteinaceous
124 macromolecules (*e.g.* whey protein microgels) alone can be used to replace food
125 polysaccharides in a tribological context remains unknown. The latter might be more
126 difficult because of the complex non-Newtonian rheology of such polysaccharides -
127 showing extreme shear-thinning behaviour, even at shear rates ($\dot{\gamma}$) above 10^5 s^{-1}
128 (Stokes, 2011), which is of the order of $\dot{\gamma}$ that can occur between the tribological
129 surfaces.

The aim of this study was to explore the capability of microgels to replace polysaccharide thickeners as lubricants in food systems. In order to assess that, we compared rheological and tribological properties of mixtures of D (at 5 wt%) + W with mixtures of WPM (at 41.7 vol%) + W at various comparable concentrations of W. Firstly, the influence of addition of D (1 - 11 wt%) to W (5 wt%) solution or WPM (41.7 vol%) dispersion on tribological and rheological behaviour of the mixtures is discussed and also compared to that of individual D, W or WPM solutions. Then, W-D conjugates and its microgelled version were investigated to explore whether such conjugation brings any novel lubricity features. D is a Newtonian polysaccharide and its conjugation to W has been well documented (Araiza-Calahorra, 2020; Sun, Yu, Yang, , 2011; Sun, Yu, Zeng, Yang, & Jia, 2011). Some of the results achieved by the conventional MTM2 tribological set up are critically assessed using the tongue-mimicked contact surfaces to understand the bio-relevance of this work to real oral processing.

2. Methods and materials

2.1 Materials

W powder (~90%) was supplied by Fonterra Limited (Auckland, New-Zealand). D (Molecular weight, M_w = 500 kDa) and 4-(2-hydroxyethyl)-1-piperazineethanesulfonic acid (HEPES) were purchased from Fisher Scientific, UK and ITW Reagents, UK, respectively. Potassium bromide (KBr, >99%) and Sorbitan oleate (Span® 80) were purchased from Sigma-Aldrich, UK. Milli-Q water with a resistivity of 18.2 MΩ.cm at 25 °C (Millipore Corp., Bedford, UK) was used as the aqueous phase for preparation of the buffer and dispersions. Sodium azide (0.05 wt%) was employed as an

antimicrobial agent. Ecoflex™ 00-30 (Smooth-On, USA) was purchased from Amazon, UK. The chemicals were used as received with no further purification.

2.2 Methods

A solution of 10 mM HEPES at pH 7.0 was used as a buffer solution for all dispersions except for W-D conjugate dispersions. For the latter, a higher ionic strength was required to compensate for a tendency for the pH to decrease during conjugation and hence a 50 mM HEPES buffer was used.

2.2.1 Preparation of WPM-containing dispersions

A solution of 12.0 wt% W in 10 mM HEPES buffer (pH 7.0) was prepared at room temperature ensuring complete dissolution of the W. Corrections were made with reference to the actual protein concentration of the powder (~90%) in calculating the final concentration of W (*i.e.* 12 wt%). The solution was heat treated at 90 °C for 1 h using a water bath to promote crosslinking of the protein (Sarkar, 2017). The heat-set W gel (WPG) was cooled down for 15 min under running cold water and stored at 4 °C overnight. The WPG was broken down into macroscopic gel fragments using a hand blender (Bosch MSM6B150GB, UK; at 12500 rpm for 60 s) in 10 mM HEPES buffer (pH 7.0) with a weight ratio of 1.4:1 (HEPES:WPG). The dispersion of WPG fragments in HEPES solution was degassed (Intertronics, Thinky ARE-250) and passed twice through a custom made Jet Homogenizer (Jet Homogenizer, University of Leeds, UK (Sarkar, 2017)) operating at a pressure of 300 ± 20 bar (Sarkar, 2017). The dispersion of whey protein microgel particles in HEPES buffer after jet homogenization is referred to as WPM hereafter. The volume fraction of WPM in the dispersion was estimated as ~ 41.70% (Sarkar, 2017) from the initial mass (volume) of WPG and the volume of buffer in which it was dispersed. This assumed negligible

swelling of the microgels upon dilution. For WPM + D and WPM + W samples, a pre-calculated amount of D or W was dissolved in the buffer just before shearing the WPG with the hand blender to obtain dispersions of WPM + D[1], WPM + D[5] and WPM + D[11] or WPM + W[1], WPM + W[3] and WPM + W[8]. The numbers 1, 5 and 11 in brackets indicate the [D] (wt%) in the total weight of the dispersions, respectively. Likewise the numbers 1, 3 and 8 in brackets denote the approximate [W] (wt%) in the total weight of the dispersions, respectively. The [W] (wt%) in HEPES buffer (*i.e.*, the free water; excluding the water trapped in the cross-linked network of WPM) are shown in Table S1, which were 1.06, 5.59 and 13.27 respectively. Since, D[5] and WPM (41.7 vol%) showed identical shear viscosity value (η) at $\dot{\gamma} = 2000$ s^{-1} (η_{2000}) (see Results section), these two systems were ideal for comparison. A summary of naming and coding of all the samples prepared in this study is shown in Table 1.

Table 1. Sample nomenclature specifying the composition of the dispersions.

Family of samples	Sample name	Dextran (wt%)‡	Whey protein (wt%)‡	Whey protein microgel (vol%)‡
Biopolymer	D[1]	1	-	-
	D[5]	5	-	-
	D[11]	11	-	-
	W[5]	-	5	-
Biopolymer mixture	D[1] + W[5]	1	5	-
	D[5] + W[1]*	5	1	-
	D[5] + W[5]*	5	5	-
	D[5] + W[11]*	5	11	-
	D[11] + W[5]	11	5	-
Microgel + biopolymer mixture	WPM	-	-	41.7
	WPM + W[1]*	-	0.62	41.7
	WPM + W[3]*	-	3.26	41.7
	WPM + W[8]*	-	7.74	41.7
	WPM + D[1]	1	-	41.7
	WPM + D[5]	5	-	41.7
	WPM + D[11]	11	-	41.7
Conjugate	Conj(D[11] + W[5])	11	5	-
Conjugate microgel	Conj(D[11] + W[5])MG	11	5	41.7

‡ The values represent the concentrations of the relevant biopolymers (pristine or conjugated) in the total weight/ volume of the dispersions.

* The concentration of whey protein in free water (*i.e.* water content excluding WPM or D) can be found in Table S1.

2.2.2 Preparation of W-D conjugated dispersions

Maillard conjugation was promoted via the method described by Araiza-Calahorra et al. (Araiza-Calahorra, 2020) with a slight modification. D and W (2:1 w/w) were mixed in 100 mL of Milli-Q water at room temperature. The pH of the mixture was adjusted to pH = 8.0 before freeze drying for at least 48 h. The freeze dried powder was placed in a humidity-controlled glass desiccator and incubated in an oven at 60 °C. The desiccator was preheated to 60 °C before introducing the powder. A relative humidity of ~80% was obtained using a saturated KBr solution. The powder was incubated for 48 h to induce the Maillard reaction (Araiza-Calahorra, 2020). The conjugated powders were stored in a dry desiccator before further use and analysis. The dispersion of W-D conjugate (that is, Conj(D[11] + W[5])) was prepared via dissolution of its powder in 50 mM HEPES to a [W] = 5 wt% (conjugated and non-conjugated) and [D] = 11 wt%. For the microgels of W-D conjugate, referred to as Conj(D[11] + W[5])MG, a conjugate solution equivalent to 10 wt% whey protein was prepared and thermally cross-linked at 65 °C for 1 h. The gel obtained was mixed with 50 mM HEPES at 1:1 w/w, fragmented with the hand blender followed by two passes through the Jet Homogenizer at 300 ± 20 bar. Conjugation influences the extent of protein unfolding and hence the subsequent gelation process (Sun, Yu, Yang, , 2011). In our case the temperature of 90 °C used to generate the WPG could not be used for gelation of the W-D conjugates because this temperature led to the formation of a very stiff gel that was too difficult to break down into microgel particles via the above methodology. Possibly this was due to the unconjugated dextran chains within the gel matrix acting as reinforcing fibres within the composite and enhanced rate of denaturation and

aggregation of glycosylated protein chains, as compared to unconjugated protein (Sun, Yu, Yang, , 2011).

2.2.3 Preparation of non-microgelled dispersions

The biopolymer solutions of dextran (D[1], D[5], D[11]), whey protein isolate (W[5]), and mixtures of dextran and whey protein (D[1] + W[5], D[5] + W[1], D[5] + W[5], D[5] + W[11], D[11] + W[5]) were produced by mixing the D and W at the concentrations denoted in brackets under magnetic stirring at room temperature (22 °C) at least for two hours until a homogenous dispersion was obtained.

2.2.4 Preparation of 3D-tongue-mimicking elastomeric surfaces

The 3D-tongue-mimicking surfaces were developed based on previously published work (Andablo-Reyes, 2020). A code was developed using Matlab (MathWorks, USA) to randomly place 200 filiform-shaped cylindrical rods of 250 μm height and 175 μm radius, plus 20 fungiform-shaped hemispheres of 500 μm height and 500 μm radius on a unit cell of 1 cm^2, based on a spatial Poisson point distribution, defined by equation (1):

$$Pa(X = n) = \frac{\lambda^n e^{-\lambda}}{n!} \quad (1)$$

where, X is the random variable representing the number of points in a defined area and λ is the rate of the distribution reflecting the expected number of points in the area. This distribution informed the x and y coordinates for the fungiform and filiform 'papillae' on the master mould.

AutoCAD® (Autodesk, 2020, USA) was used to generate drawings of the above master mould of simulated papillae-containing surfaces. The AutoCAD drawing was 3D printed on an acrylic resin (Perfactory® HTM140) using a Perfactory 3D Printer (EnvisionTEC, Dearborn, USA) to produce a negative master mould. The 3D-tongue-mimicking surface was produced via a soft-lithographic process from the master mould. A solution of Ecoflex + 0.05 wt% Span 80 was degassed (Intertronics, Thinky ARE-250) and casted onto the polyvinyl alcohol(PVA)-treated master mould made of the acrylic resin (Perfactory® HTM140) (Andablo-Reyes, 2020). The solution was cured at room temperature for at least 5 h and the elastomeric replica (positive impression) was peeled off the mould. The replica was sonicated in isopropyl alcohol (IPA) and deionized water for 10 and 20 min, respectively, to remove traces of PVA and contamination before tribological testing. These soft elastomeric samples contained the random spatial distribution of filiform and fungiform papillae based on the characterization of size and distribution of papillae in a real human tongue mask (Andablo-Reyes, 2020).

2.2.5 Particle size measurements

The hydrodynamic diameter (d_H) of the microgel particles was measured using a Zetasizer (Ultra Zetasizer, Malvern Panalytical) via dynamic light scattering (DLS) at 25 °C. The microgel-containing dispersions were diluted using HEPES buffer (pH 7.0) at a volume ratio of 1 : 99 (dispersion : HEPES) and dispersed in an ultrasonic bath at least for 15 min before measurements. Approximately, 1 mL of the diluted dispersion was pipetted into a polystyrene cuvette and scattered light detected at 173°. A refractive index of 1.54 for microgels and viscosity of 8.9×10^{-4} Pa s (i.e., that of pure

268 water) for aqueous medium were assumed. At least three replicates using three
269 separate samples were conducted and the data were averaged (n = 3 × 3).
270
271 ***2.2.6 Bulk rheological measurements***
272 Rheological experiments were conducted using a modular compact rheometer (MCR
273 - 302, Anton Paar, Austria). The η was measured via cone-on-plate (CP50-1, angle
274 1°) geometry at 37 °C (to mimic oral physiological temperature). Viscosity results were
275 measured at an initial value of $\dot{\gamma}$ = 1 s^{-1}, ramped logarithmically and terminated at 2000
276 s^{-1} (i.e., increasing order of $\dot{\gamma}$). Five data points were recorded within each decade of
277 the measurement range. At each $\dot{\gamma}$, a minimum 30 s window was set to achieve stress
278 stability. The measurements were comprised of six steps. The samples were
279 sonicated before measurements for at least 5 min, left stationery on the rheometer
280 plate for 30 s before a pre-shear step at $\dot{\gamma}$ = 500 s^{-1} for 120 s to hinder aggregation.
281 Then the sample was left for 60 s to achieve a steady state immediately before the
282 shear rate ramp. Lastly, to check for hysteresis, after the viscosity measurements a
283 120 s interval of steady state was applied and a viscosity measurement was taken at
284 $\dot{\gamma}$ = 500 s^{-1} immediately after. The hysteresis was negligible for all samples. Silicone
285 oil, in combination with a thermo-control hood, was used to minimise the influence of
286 evaporation during measurements. At least three replicates using separate samples
287 were conducted and the data were averaged using OriginPro.
288 ***2.2.7 Tribological performance***
289 The frictional properties of the dispersions were investigated using two setups, namely
290 a MTM2 and a modified rheometer (Kinexus Ultra+, Malvern Instruments, Malvern
291 U.K.) enabling μ measurements using the afore-mentioned 3D-tongue-mimicked
292 elastomer surfaces (Andablo-Reyes, 2020).

293 The tests with MTM2 were performed in a ball-on-disk configuration at 37 °C
294 under a slide-to-roll ratio (SRR) of 0.5 and using smooth pristine polydimethylsiloxane
295 (PDMS) specimens (ball of 19 mm and disc of 46 mm diameter). The PDMS
296 specimens for MTM2 testing were supplied by PCS Instruments and had an elastic
297 modulus and surface roughness (S_a) of 2.1 MPa and 20 nm respectively (Andablo-
298 Reyes, 2019). The SRR was calculated using equation (2):
299

$$SRR = \frac{2(u_{a,X} - u_{b,X})}{u_{a,X} + u_{b,X}} \quad (2)$$

300
301 where, $u_{a,X}$ and $u_{b,X}$ are the speeds of body a and b in the *X* direction (Sarkar, 2021).
302 A load of 2 N was applied during experiments, corresponding to a Hertzian contact
303 pressure of ~200 kPa (Sarkar, Andablo-Reyes, , 2019). The μ results are presented
304 in the form of μ as a function of entrainment speed (u) or the product of the limiting
305 high-shear viscosity obtained at $\dot{\gamma} = 2000$ s^{-1} (*i.e.* η_{2000}) and the u (*i.e.* $\eta_{2000} \times u$),
306 determined as described below (Sarkar, 2021). The friction forces were measured in
307 order of increasing speed, at $10^{-3} < u < 2$ m s^{-1}. An extensive sample cleaning
308 procedure was applied between each experiment to eliminate the influence of surface
309 contamination which briefly included sonication steps in sodium dodecyl sulphate (2
310 wt% in DI water), IPA and DI water for 10 min at each step. At least three replicates
311 using separate samples were conducted and the data were averaged.
312 Tribology of the samples were also tested using a biomimetic tongue surface
313 emulating the stiffness, roughness and hydrophilicity of a real human tongue, the
314 testing procedure is detailed previously (Andablo-Reyes, 2020). Briefly, a sample of
315 the elastomer surface (i.e. Ecoflex™ 00-30 + 0.05 wt% Span 80, Young's modulus of
316 130 KPa - cut to 2 × 2 cm), which was 3D printed, was attached to the top plate of the

rheometer with the centreline of the sample 1.5 cm from the centre of the top plate. A normal force of 1.0 N was applied to compress the sample against a stainless steel plate embedded in a pot filled with the dispersion. The pot was a custom-designed ring made from a UV-cured polymer. Tests were conducted at 37 °C in pure-sliding and unidirectional rotary tribocontact. Similar to tests with the MTM2, sliding was employed in the order from low (5×10^{-5} m s^{-1}) to high (9×10^{-3} m s^{-1}) u values by increasing the angular velocity from 0.005 to 1 s^{-1}. For each sample a complete 2π rad rotation was applied at each velocity before a torque (τ) was recorded. The τ was used to calculate the corresponding μ via equation (3):

$$\mu = \frac{\tau}{rF} \tag{3}$$

where, F is the normal load (1 N) and r is the radius of the top plate (0.025 m). Each dispersion was assessed by two readings on three separate elastomeric specimens and lubricant samples (n = 3 × 2).

2.2.8 Statistical analyses

All measurements were done three times on triplicate samples prepared on separate days and are reported as the mean and standard deviation (n = 3 × 3) unless otherwise specified. The statistical analyses were conducted using one-way (ANOVA) and the significant difference between samples were considered when $p < 0.05$ using Tukey test.

3. Results and discussion

3.1 Size of WPM in different dispersions

The measured hydrodynamic sizes of the WPM particles in various dispersions are presented in Table 2. All samples showed monomodal size distributions (shown in Figure S1). Microgels showed polydispersity indices (obtained from correlation data via cumulants analysis) between 0.18 and 0.27 satisfying the analyses (Table 2). For non-conjugated dispersions (mixtures of WPM and D or W), the d_H ranged between 94 ± 5 and 135 nm ± 2 (Table 2) assuming the microgels were spherical, justified by previous transmission electron microscopy (Sarkar, 2016). The size results for WPM particles are in agreement with the data previously reported for WPM particles produced under similar experimental conditions (Andablo-Reyes, 2019). Addition of W to WPM at different [W] did not influence the d_H ($p > 0.05$) (Table 2). An increase of only 10 to 20 nm in the d_H was observed upon presence of D in the process of microgel formation (Table 2).

Conjugation followed by microgel formation resulted in a significant change in microgel size. The remarkably larger size of Conj(D[11] + W[5])MG particles (Table 2) might be attributable to the lower protein-protein crosslinking density that is possible when W is conjugated to D (Sun, Yu, Yang, , 2011), resulting in a more open gel structure that might lead to greater swelling of the microgel particles when formed from the parent gel. On the other hand, the W-D conjugate gels have been shown to have elastic moduli of up to 5 times greater than that of the corresponding W gel (Araiza-Calahorra, 2020). As described earlier, this probably results from the higher concentration of biopolymers (dextran) within the gel matrix creating a composite gel with unconjugated D acting as reinforcing fibers. In addition to that, stiffer macrogels formed from W-D conjugates may be harder to break down to small microgel particles.

Table 2. Mean hydrodynamic diameter (d_H) and polydispersity index (PDI) of various whey protein microgel dispersions with or without the addition of biopolymers, measured at pH 7.0 and 25°C via *DLS*.

Sample	WPM	WPM + D[1]	WPM + D[5]	WPM + D[11]	Conj(D[11] + W[5])MG	WPM + W[1]	WPM + W[3]	WPM + W[8]
d_H (nm)	115 ± 7^{a,c}	124 ± 9^{a,c}	125 ± 11^{a,c}	135 ± 2^{a}	227 ± 1^{b}	115 ± 1^{a,c}	94 ± 5^{c}	99 ± 21^{a,c}
PDI	0.234 ± 0.015	0.233 ± 0.005	0.236 ± 0.002	0.258 ± 0.006	0.185 ± 0.002	0.223 ± 0.001	0.267 ± 0.036	0.267 ± 0.036

3.2 Bulk rheological measurements

The η of solutions of dextran (D[1], D[5], D[11]), WPM, W[5], W[5] mixtures with D[1] or D[5] or D[11], and Conj(D[11] + W[5]) are shown in Figure 1A. D is well-known to possess Newtonian properties (Carrasco, Chornet, Overend, & Costa, 1989; Sun, Yu, Yang, , 2011; Tirtaatmadja, Dunstan, & Boger, 2001) up to at least 30 wt% and M_w of 2×10^6. Average η values across the measured $\dot{\gamma}$ for D[1], D[5] and D[11] were 1.2, 9.9 and 38.2 mPa s respectively (Figure 1A). These are close to values of 1.52, 6.18 and 22.70 mPa s at 25 °C reported for dextran with a M_w of 5.31×10^5 at concentrations of 1, 4.7 and 9.5 wt%, respectively (Carrasco, 1989). In general, the viscosities of dextran solutions are expected to increase with higher M_w and concentration (Carrasco, 1989; Tirtaatmadja, 2001), corroborating our findings. Log η versus log [D] (see Figure S2 in Supporting Information) showed a slope of 1.4, which is the same as reported by Tirtaatmadja et al. (Tirtaatmadja, 2001). This shows that D[11] (the highest concentration in this study) was below the critical overlap concentration (Yang, 2020), suggesting a random-coil branched configuration with long side-chains in its branches.

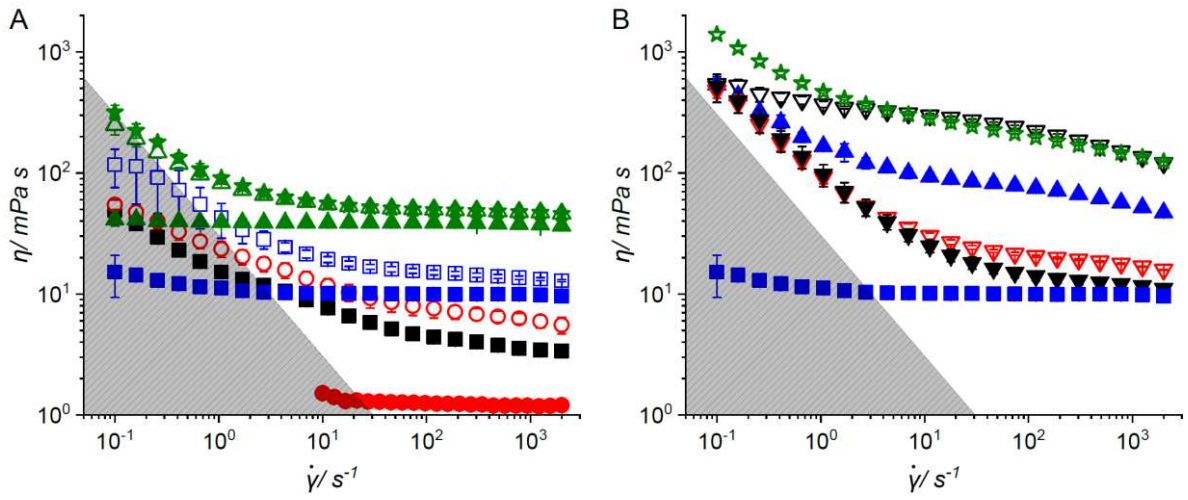

Figure 1. (A) Flow curves of the biopolymer solutions, *i.e.* dextran solutions D[1] (●), D[5] (■) and D[11] (▲); whey protein solution W[5] (■), mixtures of dextran and whey protein solutions D[1] + W[5] (○), D[5] + W[5] (□), D[11] + W[5] (△), and the conjugate Conj(D[11] + W[5]) (★). (B) Flow curves of the microgel systems WPM (▼), WPM + D[1] (▽), WPM + D[5] (▲), WPM + D[11] (▽), and the conjugated microgel Conj(D[11] + W[5])MG (☆), plus the D[5] (■), result from (A) is also shown for comparison. The shaded-hatch region in the curves denotes the invalid data range due to the geometrical limitations of the rheometer. Means are calculated based on readings on at least triplicate samples (n ≥ 3).

Whey protein solutions may show non-Newtonian behaviour (Rao, 2014) depending on the [W] and pH (Dissanayake, Ramchandran, & Vasiljevic, 2013), attributed to shear-induced rupture of inter-particle/molecular bonds or non-destructive alignment of the globular structure of whey protein with the flow direction. In our measurements, W[5] showed a moderate shear-thinning behaviour with η dropping from 10.5 mPa s at $\dot{\gamma} = 4$ s^{-1} to 3.4 mPa s at $\dot{\gamma} = 2000$ s^{-1}. The η at $\dot{\gamma} = 2000$ s^{-1} almost seemed to plateau (Figure 1A), indicating minimal protein-protein interactions occurring between W molecules. The limiting high-shear viscosity can be used to

404 estimate the hydrodynamic forces in tribological studies (de Vicente, Stokes, & Spikes,
405 2005; Sarkar, 2021; Selway, Chan, & Stokes, 2017). The η_{2000} values were used in
406 this study to normalise $\mu - u$ plots to the influence of viscous forces (discussed later).
407 All mixtures of W[5] + D exhibited shear thinning in the lower values of $\dot{\gamma}$ with
408 their η appearing to level off at the highest $\dot{\gamma}$ values (Figure 1A). The addition of W
409 slightly increased η_{2000} of D[1] + W[5], D[5] + W[5] and D[11] + W[5] dispersions (5.5,
410 12.9 and 46.2 mPa s respectively) with their viscosities approaching to that of the
411 corresponding D solutions alone, except for D[1] + W[5]. Increased [D] in solutions of
412 D + W[5] shifted the onset of Newtonian behaviour to lower $\dot{\gamma}$ values (Figure 1A). The
413 much larger molecular volume of D (Carrasco, 1989; Tirtaatmadja, 2001) means that
414 D is expected to dominate the η behviour, promote steric hindrance and disrupt inter-
415 particle/molecular interactions between W molecules. Hence significant shear thinning
416 only appears at lower $\dot{\gamma}$ in the mixtures, where there is more time for W molecules to
417 rearrange and interact. As it can be seen in Figure 1A, Conj(D[11] + W[5]) showed an
418 identical shear-thinning behaviour to that of D[11] + W[5]. This is probably a result of
419 the low degree of conjugation (< 20%) under the conditions used (Araiza-Calahorra,
420 2020) which essentially suggests the dominance of free D and W on the shear flow
421 behaviour of Conj(D[11] + W[5]) dispersion.
422 Figure 1B presents η of WPM, WPM + D[1], WPM + D[5], WPM + D[11], and
423 Conj(D[11] + W[5])MG dispersions. The most intense shear-thinning behaviour was
424 observed for WPM, showing an almost 50-fold decrease in η across the measurement
425 window, with $\eta_{2000} = 11$ mPa s. The high shear-thinning behaviour of WPM has been
426 discussed elsewhere (Andablo-Reyes, 2019; Sarkar, 2017). We note that η_{2000} of
427 WPM was over three-times greater than that of W[5] (Figure 1B). The addition of D to
428 WPM (WPM + D) significantly enhanced the resultant η across the measured $\dot{\gamma}$

values, particularly at $\dot{\gamma}$ > 100 s^{-1}, which is caused by the existence of higher overall concentration of biopolymers in the dispersed phase. Among WPM + D dispersions, a high shear-rate plateau was achieved for WPM + D[1] displaying a $\eta_{2000} = 15.9$ mPa s. With increased [D], the shear thinning behaviour of WPM + D at low $\dot{\gamma}$ values was attenuated. However, unlike with mixtures of D + W[5], the apparent levelling off at high $\dot{\gamma}$ values is delayed to higher $\dot{\gamma}$, i.e., the shear thinning was more uniform across the whole $\dot{\gamma}$ region. This behaviour probably results from the tendency of the WPM particles to entangle and retain their flocculated state until higher shear rates (Sarkar, 2017). The shear thinning of the WPM + D mixture thus represents a hybrid of the behaviour of the individual components.

In order to assess, in more detail, the influence of WPM on η of mixtures of WPM + D, in Figure 2 we plot the relative viscosity ($\eta_r = \frac{\eta_s}{\eta_D}$) of the mixtures as a function of Péclet number (*Pe*), defined in equation (4):

$$Pe = \frac{6\pi\dot{\gamma}\eta_D d_H^3}{8k_B T} \quad (4)$$

where, η_s and η_D are the viscosities of a WPM + D mixture and the corresponding D solution, respectively, whilst d_H, k_B and *T* are the hydrodynamic diameter of the WPM particles, Boltzmann constant and temperature, respectively. Figure 2 more clearly illustrates the influence of WPM on η of the WPM + D mixtures, *i.e.*, η_r > 1 across all mixtures and *Pe* number. WPM and WPM + D[1] showed an identical shear-thinning behaviour and showed a tendency to plateau at *Pe* ≈ 1, indicating similar characteristic times for flow and Brownian diffusion processes (Andablo-Reyes, 2019).

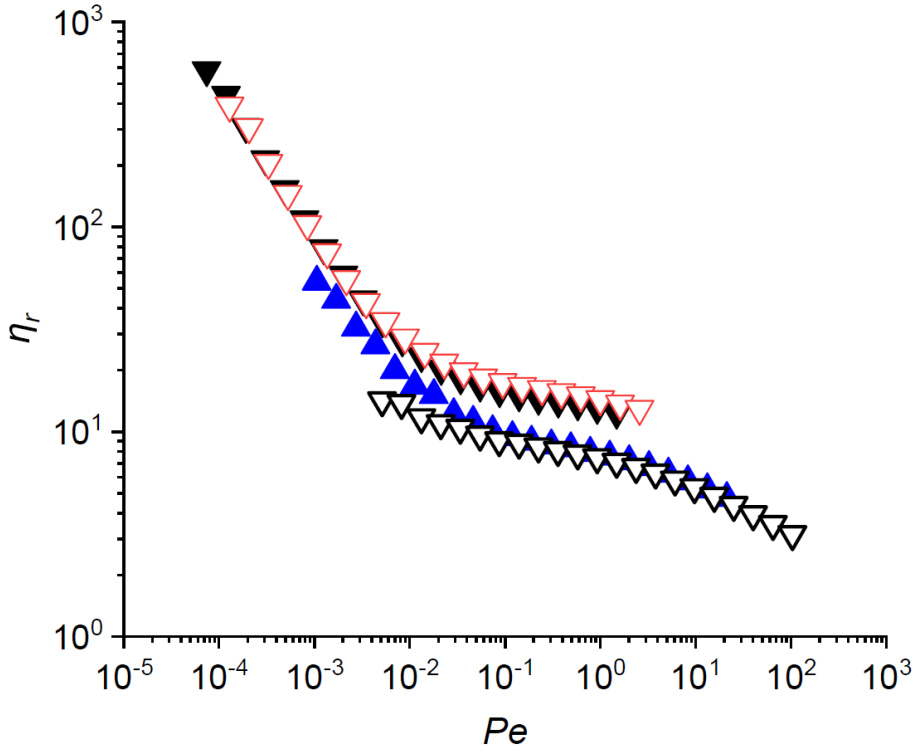

Figure 2. Relative shear viscosity of mixtures of microgel and dextran solutions WPM (▼), WPM + D[1] (▽), WPM + D[5] (▲) and WPM + D[11] (▽) as a function of Péclet number (*Pe*).

At *Pe* < 0.01, where diffusive transport should dominate, η_r showed a similar behaviour for WPM + D[5] and WPM +D[1] (or WPM alone). At *P*e > 0.1 the behaviour of WPM + D[5] and WPM + D[11] were identical, up to *Pe* as high as 10^2. Thus at low $\dot{\gamma}$ and [D] values the interactions between the WPM particles dominate the η, but at higher $\dot{\gamma}$ and [D] values the η is increasingly dominated by the background η of the D solutions. Higher [D] presumably helps to disturb the diffusive and flow behaviour of WPM particles resulting in lower η_r values at low $\dot{\gamma}$ (disrupted interactions) and delayed Newtonian plateaus at high $\dot{\gamma}$ respectively.

3.3. Soft tribology

3.3.1 Frictional behaviour of biopolymers, microgels and conjugated systems

The μ results obtained using the MTM2 for biopolymer solutions of D and W, mixtures of D and W[5], WPM, mixtures of WPM and D and conjugated systems are shown in Figures 3A and 3B.

Biopolymers. In agreement with the previous findings (Kew, Holmes, Stieger, & Sarkar, 2021; Zembyla, 2021), W[5] decreased the boundary μ from just over 1 (buffer) to 0.3 (Figure 3A and Figure S3), which suggests adsorption-induced lubricity at the interface, as schematically shown in Figure 4. Theoretically, the boundary regime specifies the complete exclusion of a continuous lubricant film from the contact interface, although local regions of trapped lubricant can exist between soft tribocontacts (Dowson, 1995). The boundary regime is usually taken as the (low) u range at which the μ becomes relatively independent of u, with some variations induced by the lubricant/ material viscoelasticity (Sarkar, 2021; Selway, 2017). The lubrication regimes are often determined qualitatively from the $\mu - u$ graphs.

In general, there is no concrete consensus on the interplay between the extent of surface adsorption and the boundary lubrication behaviour (Sarkar, 2021; Stokes, 2011). However, deposition of soft biopolymers at the interface can alleviate direct surface interactions between contact bodies (asperity-asperity contact) in the boundary regime or via reducing hydrophobic interactions in self-mated PDMS contacts (Lee, Iten, Müller, & Spencer, 2004), hence reducing the boundary μ.

D[1] and D[5] showed a similar boundary μ to that of the buffer (Figure 3A and Figure S3A), which is in line with previous findings for steel-on-glass (Perrino, 2009) and PDMS-on-steel tribocontacts (Käsdorf, et al., 2017). The lack of propensity of dextran to prompt hydrophobic and/or electrostatic interactions with PDMS surfaces

(Käsdorf, 2017; Perrino, 2009) led to an unfavourably high boundary μ. Note that D[11] has not reach the boundary regime in the MTM2 measurements.

Upon increase of [D], the onset of the elasto-hydrodynamic lubrication (EHL) regime (*i.e.* full-separation of contact-bodies by a thin fluid film at the interface) shifted to lower u values (Figure 3A). This shift is a result of the increased η values of the dispersions, as shown in Figure 1A. The minimum u at which the EHL regime was established (u_{EHL}), which is associated with the speed at which the minimum friction coefficient (μ_{min}) is often observed, decreased by over an order of magnitude, from ~1 to 0.1 m s^{-1}, when the [D] was increased from 1 to 11 wt%. The shift was significant enough to impede the boundary regime at the lowest u measurable (1 mm s^{-1}) via the MTM2. This emphasizes the viscous lubricity of D, especially at [D] = 5 and 11 wt%. This is schematically shown in Figure 4, where viscous-driven hydrodynamic forces generate a lifting force *(F_v in Figure 4)* which enhances the gap between contacting surfaces. The viscous lubricity of D can also be appreciated in Figure S3A (Supporting Information), where the μ curves for D[1], D[5] and D[11] collapsed onto a single curve.

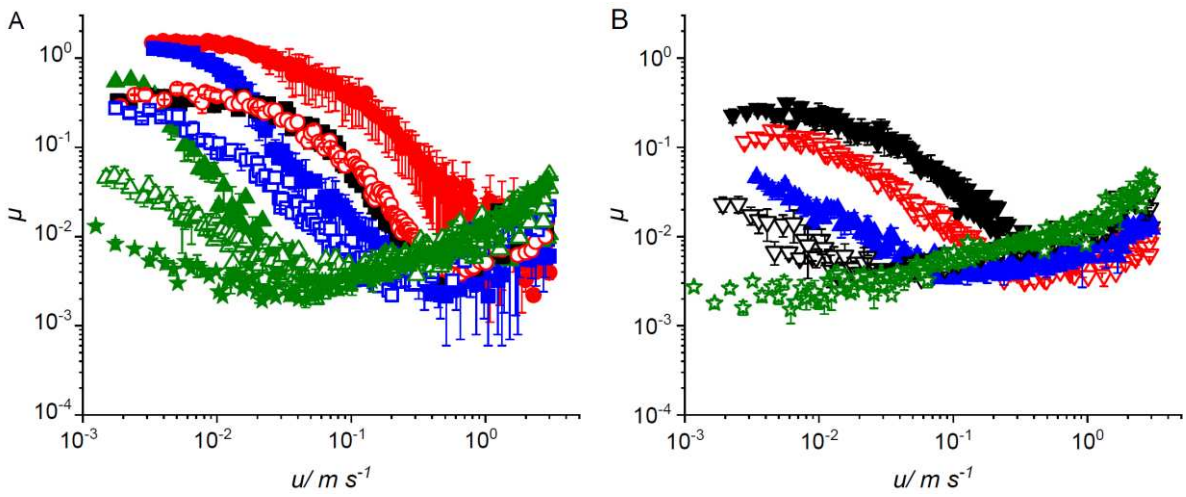

508

509 **Figure 3.** (A) Friction coefficient (μ) *versus* entrainment speed (u) for biopolymer
510 solutions D[1] (●), D[5] (■), D[11] (▲) and W[5] (■); mixtures of dextran and whey
511 protein D[1] + W[5] (○), D[5] + W[5] (□), D[11] + W[5] (△) and also the conjugate
512 Conj(D[11] + W[5]) (★). (B) μ *versus* u for the microgel systems WPM (▼), WPM +
513 D[1] (▽), WPM + D[5] (▲), WPM + D[11] (▽), and also conjugated microgel
514 Conj(D[11] + W[5])MG (☆). Means are calculated based on readings on at least
515 triplicate samples (n ≥ 3).

516

517 ***Biopolymer mixtures.*** The addition of D[1] and D[5] to W[5] gave marked
518 changes to the boundary μ of W[5] (Figure 3A). This is further evidenced in Figure
519 S3A (Supporting Information) which show the $\mu - \eta_{2000}u$ plots. It is known that
520 hydrophilic neutral coatings can possess anti-fouling properties against protein
521 adsorption (Österberg, et al., 1995). Dextran is part of that category and the anti-
522 fouling characteristics of dextran-coated surfaces (Griesser, et al., 2002; Perrino,
523 2008) or modified-dextran layered surfaces (Martwiset, Koh, & Chen, 2006; McLean,
524 et al., 2000; Piehler, Brecht, Hehl, & Gauglitz, 1999) are well-documented. Therefore,
525 the same boundary μ observed for W[5], D[1] + W[5] or D[5] + W[5] indicates the

limited adsorption behaviour of D on PDMS, and addition of D to W does not influence the surface-driven lubrication performance of the latter. This suggests that frictional forces in direct surface contacts for D[1] + W[5] and D[5] + W[5] were mainly governed by W adsorbing to the PDMS surfaces.

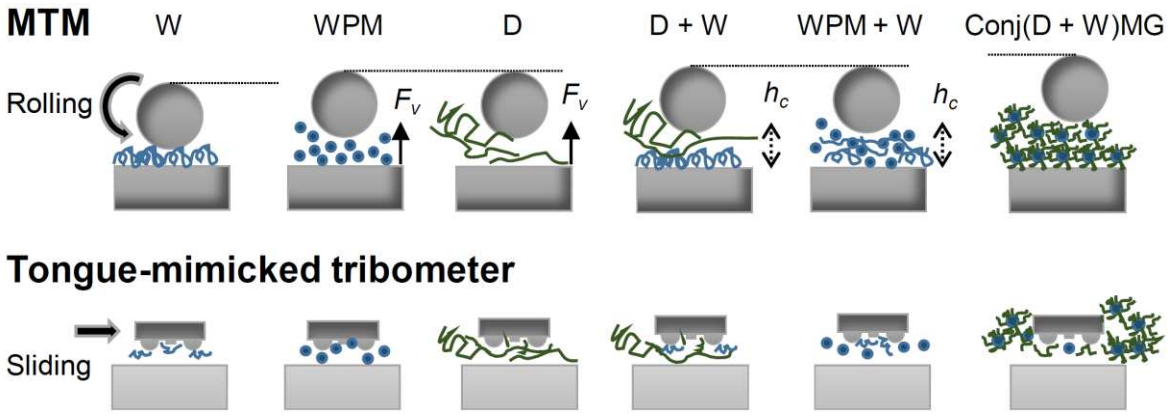

Figure 4. Schematic illustration of governing lubrication mechanisms of the studied dispersions in MTM and 3D tongue-mimicked tribocontacts. Adsorption and probable aggregation of W provided thin-film and hydration lubricity. F_v is the lifting force generated by hydrodynamic/ viscous forces (lubricant viscosity) when D or WPM was added to the system. The central film thickness values (h_c) for each pair of systems: D[5] + W[1] and WPM + W[1], D[5] + W[5] and WPM + W[3], and D[5] + W[11] and WPM + W[8], were almost identical as a result of the similar thickening behaviour of WPM and D[5]. The entrainment of Conj(D[11] + W[5])MG particles into the contact interface facilitated cushioning and brush lubrication mechanisms in the MTM measurements, a factor that was lacking in the tongue-mimicked tribocontacts.

Comparing the solutions of D to its mixtures with W[5], it can be seen that W[5] does not influence u_{EHL} of the mixtures considerably (Figure 3A), particularly when the [D] was greater than [W], showing W's trivial viscous-lubricity behaviour. The addition

535 of W[5] to D solutions contributed to the lubrication performance of the mixtures in the
536 mixed regime (clearly reflected in Figure S3A, Supporting Information), where the μ
537 increases monotonically with decreasing u until it reaches a plateau (*i.e.* the boundary
538 regime). This can be attributed to W adsorption and its contribution to the slight
539 increase in η of the dispersions (Figure 1A), though the former is expected to be the
540 dominant factor. In the mixed lubrication regime, the contact surfaces are in close
541 proximity, leading to direct contact of surface asperities whilst a part of the contact
542 load is still borne by the confined fluid (Sarkar, 2021). Therefore, adsorbed layers can
543 still play a role in the mixed regime (Sarkar, 2021) either by lowering the extent of
544 asperity-asperity contacts (Stokes, 2011) and/or by facilitating hydration lubrication
545 (Hu, Andablo-Reyes, Soltanahmadi, & Sarkar, 2020; Klein, 2013; Xu, et al., 2020) via
546 an easy-slip layer (Figure 4).

547 ***Conjugate.*** Interestingly, the conjugate (Conj(D[11] + W[5])) showed a lower
548 mixed μ as compared to D[11] + W[5] (Figure 3A), despite their almost identical η_{2000}
549 (Figure 1A). When D and W (or WPM) are mixed without heat treatment - except for
550 hydrogen bonding - electrostatic interactions, complex formation and conjugation are
551 not expected due to the neutral nature of D (Sun, Yu, Yang, , 2011). However,
552 glycosylation of protein molecules is known to bring about a loss of secondary
553 structure and to mitigate heat-induced aggregation (Sun, Yu, Yang, , 2011).

554 Flash-heating is a well-known phenomenon in the tribology of solid surfaces
555 and refers to local heating of the contact interface in the event of asperity-asperity
556 contacts under high shear (the mixed and boundary regime). The local heating can be
557 significantly higher than the temperature of the bulk lubricant (Vakis, et al., 2018), with
558 important implications for friction (*e.g.* can lead to phase transformation of hard
559 metals). The literature in relation to flash-heating in oral soft tribology is scarce,

probably due to the low temperatures assumed (often 37 °C, emulating physiological conditions) and complexities around viscoelastic energy dissipation (Persson, 2006). The surface roughness, contact geometry and viscoelastic properties influence the lubricant squeeze-out dynamics and hence the μ (Lorenz, et al., 2013). With flash-heating altering local viscoelastic (asperity level) properties of an elastomer, the squeeze-out dynamics are expected to significantly differ when the elastomer encounters flash-heating. Although the impact of flash-heating on structural change of the surface adsorbed films is usually overlooked, similar concepts on lubricant film collapse have been raised and referred to as 'de-wetting' at the asperity level (Selway, 2017). PDMS has a thermal conductivity of around 0.16 W mK^{-1}, at least two orders of magnitude lower than that of the bearing steel (AISI 52100) (Reddyhoff, Schmidt, & Spikes, 2019), and thus could undergo a local heating much more easily and within a relatively short period of time when the sliding speed is high enough to make the thermal diffusion negligible (reported to be sliding speed > 0.01 m s^{-1} for *the* rubber (Persson, 2006)).

Considering all the above, we propose that in the event of flash-heating, W-D conjugate molecules will resist aggregation, bringing about a slower rate of de-wetting. Our hypothesis is that, the loss of secondary structure and reduced heat-induced aggregation of Conj(D[11] + W[5]) (Sun, Yu, Yang, , 2011), results in a stacked arrangement of such molecules, aligned parallel to the fluid flow. This will generate a slip plane in which the relative motions of biopolymer chains can dissipate the interfacial frictional stresses. Consequently, the conjugated system (Conj(D[11] + W[5])) shows a considerably lower μ (at $u < 3 \times 10^{-2}\ m\ s^{-1}$) compared to D[11] + W[5] (Figure 3A). The susceptibility to aggregation of W in the non-conjugated systems (*i.e.* D mixtures with W[5]) in the event of flash-heating may hinder the formation of the

585 proposed stacked arrangement and/or lead to faster fluid squeeze-out as compared
586 to Conj(D[11] + W[5]).

587 ***Microgel systems.*** Figure 3B presents the μ results for WPM and its
588 dispersion in dextran solutions (WPM + D[1], WPM + D[5], WPM + [11]), and
589 Conj(D[11] + W[5])MG system. In order to achieve a valid comparison, the WPG for
590 all dispersions (except for the Conj(D[11] + W[5])MG) was always prepared from W
591 alone, since D is shown to influence the gelation behaviour of W (Araiza-Calahorra,
592 2020; Sun, Yu, Yang, , 2011; Sun, Yu, Zeng, , 2011). The lubrication behaviour of
593 whey protein microgels has been previously assessed via the MTM2 to show its
594 influence on μ across the mixed and boundary lubrication regimes (Andablo-Reyes,
595 2019; Sarkar, 2017).

596 In this work, WPM performed similarly to W[5] in the boundary regime (Figure
597 3B) implying that the adsorbed/trapped layers of whey protein microgel and non-
598 denatured whey protein molecules provided very similar interfacial effects (Figure 4).
599 Interestingly, the u_{EHL} for WPM and W[5] occurred at a similar value (~ 0.4 m s^{-1})
600 despite the fact that the η_{2000} of the WPM was over three times larger than that of W[5]
601 (Figure 1). To investigate this observation further, the lubricant film thicknesses and
602 the $\dot{\gamma}$ values at the contact interface in the EHL regime were estimated as follows. The
603 central film thickness (h_c) of the microgel-containing dispersions was calculated using
604 the modified Hamrock-Dowson empirical expression (Hamrock & Dowson, 1978;
605 Myant, Fowell, Spikes, & Stokes, 2010):
606

$$h_c = 3.3R'U^{0.63}W^{-0.13} \quad (5)$$

where, U is the dimensionless speed parameter ($\frac{u\eta_{eff}}{R'E'}$) and W is the dimensionless load parameter ($\frac{F}{E'R'^2}$). The terms η_{eff} and F are the effective η of the fluid at the extant shear rates relevant to tribological contact (often taken as the second Newtonian plateau in rheological measurements (de Vicente, 2005), η_{2000} in this study) and the applied normal load. R' and E' are the effective radius of curvature in the direction of the fluid entrainment and the equivalent modulus of elasticity of PDMS specimens, respectively (Sarkar, 2021). R' and $E'$are given by $\frac{1}{R'} = \frac{1}{R_1} + \frac{1}{R_2}$ and $E' = \frac{2E_1E_2}{E_1(1-\nu_2^2)+E_2(1-\nu_1^2)}$ where, (E_1 and E_2), (ν_1 and ν_2) and (R_1 and R_2) are the elastic moduli, Poisson's ratios and the radii of curvature of the two contact bodies 1 and 2 (*i.e.*, the ball and disc), respectively (Sarkar, 2021). Assuming laminar flow with no wall slip, a rough estimation of the $\dot{\gamma}$ can be obtained from $\dot{\gamma} = \frac{SRR.u}{h_c}$. The approximate $\dot{\gamma}$ values together with u_{EHL} and h_c for microgel-containing dispersions are shown in Table 3. The $\dot{\gamma}$ values agree with the values of over 10^3 claimed for tribological contacts (Stokes, 2013).

Table 3. Viscosities of the dispersions at $\dot{\gamma} = 2000$ s^{-1} (η_{2000}), the entrainment speeds (u_{EHL}), the calculated central film thicknesses at the contact interface (h_c) and estimated shear rates (Est. $\dot{\gamma}$) in the EHL regime.

Dispersions	η_{2000} (mPa s)	u_{EHL} (m s^{-1})	h_c (μm)	Est. $\dot{\gamma}$ (s^{-1}×10^3)
WPM	11	0.380	3.071	61.872
WPM + D[1]	16	0.250	2.963	42.192
WPM + D[5]	47	0.125	3.791	16.486
WPM + D[11]	121	0.035	3.079	5.682

Conj(D[11] + W[5])MG	124	0.001*	0.334	1.494
WPM + W[1]	12	0.376	3.327	56.512
WPM + W[3]	12	0.364	3.180	57.233
WPM + W[8]	20	0.190	2.872	33.081

* The EHL regime could not be accurately identified and a value of 0.001 was assumed as the u_{EHL}.

The estimated $\dot{\gamma}$ and h_c for WPM are 30x higher in magnitude than the highest $\dot{\gamma}$ measured with the rheometer (Figure 1) and the WPM particle size (Table 2). This suggests that at a large h_c/d_h and relatively high $\dot{\gamma}$, WPM and W[5] can show similar EHL behaviour. In other words, the impact of particles on the hydrodynamic forces are not significant and WPM can show lower η values under extreme $\dot{\gamma}$ values taking place in tribological conditions (*i.e.* $\eta_{2000} \neq \eta_{eff}$) which may prompt shear-induced deformation or de-swelling (water loss). This can be attributed to the extreme shear thinning behaviour of non-Newtonian fluids when subjected to high shear rates at the inlet of tribocontacts (Cassin, Heinrich, & Spikes, 2001).

The transition from the boundary regime to the mixed regime occurred at a lower u for WPM compared to that for W[5]. Further, the μ at $0.01 < u < 0.04$ m s^{-1} was lower for the same comparison (Figure 3B). Using equation (5), the calculated h_c and h_{min}(*i.e.* the minimum film thickness, $h_{min} = 2.8R'U^{0.68}W^{-0.20}$) at the above speed range were 0.31 to 0.74 and 0.14 to 0.36 μm, respectively. In the boundary and transition to mixed regimes, h_{min} tends to better represent the actual lubricant film thickness due to a high proportion of asperity-asperity contacts in these regimes. Interestingly, the fall in μ for WPM took effect at a u value with a corresponding h_{min} value (0.14 μm) just greater than d_H of the WPM (~0.12 μm) and the decrease continued until $h_{min} \sim 3 \times d_H$ (0.36 μm). This seems to corroborate the rolling mechanism of WPM (*i.e.* ball bearing) which leads to a μ reduction when the gap size

647 is equal or slightly larger than the particle size (Sarkar, 2017; Yakubov, Branfield,
648 Bongaerts, & Stokes, 2015). It is also worth noting that rupture of the WPM particles
649 is not expected under the contact pressure used in this study (Andablo-Reyes, 2019).
650 Thus, the structural integrity of the microgels facilitates their entrainment and reduction
651 of the μ at u values up to at least 0.04 m s^{-1}.

652 For WPM and its dispersions in dextran solutions (Figure 3B) h_c in the EHL
653 regime (2.9 to 3.8 μm) also exceeds the particle sizes (0.124 - 0.135 μm) by at least
654 an order of magnitude (Tables 1 and 3). Thus the large h_c/d_h ratios, together with high
655 $\dot{\gamma}$ values (5 - 42×10^3 s^{-1}) at the contact interfaces (breaking up any particle
656 aggregates) likewise brought about free entrainment of particles into the contact
657 region. The high η values of WPM + D[5] and + WPM + D[11] (Figure 1B) shifted u_{EHL}
658 to 0.1-0.3 $\times$ u_{EHL} of WPM, impeding tribo-contacts into the boundary regime at the
659 lowest u measurable with the MTM2 (Figure 3B and Figure S3B in Supporting
660 Information).

661 The μ of WPM + D[1] in the boundary (and mixed) regime was slightly lower
662 when compared to WPM (Figure 3B), which can be attributed to its higher η (Figure
663 1B) resulting in the lubricant film squeezing out more slowly (Selway, 2017). In soft
664 tribo-contacts, the viscoelasticity of elastomers at asperity scale can further reduce the
665 squeeze out dynamics, as discussed by Dowson two decades ago (Dowson, 1995),
666 referred to as '*micro-EHL*'. Here, deformation of the surface asperities results in
667 perturbation to the local pressure profile that can lead to a persisting lubricant film
668 between surfaces even into the boundary regime (Dowson, 1995). The lower μ with
669 the addition of D[1] to WPM was not observed for D[1] + W[5] (Figure 3A, also see
670 Figure S3B showing the $\mu - \eta_{2000} \times u$ plots). Our reasoning for this is that, adsorption
671 of W, under these conditions, would probably alter the contact surface properties

672 (wettability, roughness, chemistry and adhesiveness, etc.). This restrains or masks the
673 influence of viscosity on squeeze-out and de-wetting dynamics. As far as we are aware
674 this observation has not been addressed in the literature. Another reason might be
675 that the particulate nature of WPM microgels facilitates separation of contact bodies
676 (not forgetting that they are larger in size compared to the typical surface roughness)
677 and therefore helps to accommodate D chains between the particles and the surfaces.
678 ***Conjugate microgels.*** Conj(D[11] + W[5])MG surpassed all other dispersions
679 in lubricity showing *superlubricity* (*i.e.* resistive forces nearly vanish with friction
680 coefficients < 0.01 within severe tribo-conditions). In the presence of Conj(D[11] +
681 W[5])MG, μ was around 0.002 at $u \sim 0.001$ m s^{-1} , which significantly exceeded that of
682 WPM + D[11] despite their almost identical viscosities at $\dot{\gamma}$ > 100 s^{-1} (Figures 3B and
683 1B). Clearly the conjugate microgel particles must have some sort of different structure
684 (*e.g.* altered state of protein unfolding following conjugation (Sun, Yu, Yang, , 2011))
685 that can influence their adsorption and/or entrainment.
686 The Conj(D[11] + W[5])MG particles were larger than the WPM but still slightly
687 smaller (d_H = 0.227 μm - see Table 2) than the h_c at 0.001 m s^{-1} (0.334 μm - as shown
688 in Table 3). Considering the low $\dot{\gamma}$ occurring at 0.001 m s^{-1} (estimated as 1494 s^{-1} -
689 see Table 3), particle aggregation is more likely to persist. Therefore, we hypothesize
690 that there is a more aggregated state of these microgel particles (or condensed close-
691 packed state) at $0.001 < u < 0.01$ m s^{-1} which facilitates full separation of contact
692 bodies, alleviating the shear stress at low u via a '*cushioning*' effect, as reflected in
693 Figure 4. The surface interactions in compliant tribo-contacts of PDMS-PDMS involve
694 substantial cohesive and interfacial adhesive friction (Sills, Vorvolakos, Chaudhury, &
695 Overney, 2007) and the cushioning effect by the Conj(D[11] + W[5])MG particles will
696 significantly moderate these resistive forces by hindering hydrophobic-hydrophobic

interaction in PDMS-PDMS contacts. A similar mechanism was proposed by Sarkar et al. (Sarkar, 2017) on observation of packed WPM particles at extremely high particle fractions, bringing about μ values as low as 0.1 on hydrophobic surfaces. The *superlubricity* for Conj(D[11] + W[5])MG could also be attributed to the effect of D chains sticking out the microgels. This will facilitate '*brush-like*' lubrication. Surface adsorbed and grafted dextran (co)polymer chains have shown promising lubrication properties (Goren, 2014; Perrino, 2009; Rosenberg, 2011) depending on the polymer chain conformation and environmental parameters (e.g., pH and solvation). These various possible explanations are schematically illustrated in Figure 4 and need further testing, but it is interesting that the superlubricity of Conj(D[11] + W[5])MG observed in the MTM2 was not observed in the experiments with 3D tongue-mimicked surfaces, discussed later.

3.3.2 Comparison of frictional and flow behaviour of combined D[5] + W and WPM + W systems

The promising viscous and boundary lubricity of WPM suggested that it might be able to deliver similar viscous lubricity as non-conjugated D. It was also noted that D[5] and 41.7 vol% WPM had almost identical η_{2000} (9.9 ± 0.4 and 11.0 ± 0.7 mPa s, respectively). Therefore, we performed experiments to examine the flow (Figure 5A) and μ behaviour (Figure 5B) of W mixtures with D[5] or [WPM] = 41.7 vol%, whilst varying the [W] in free water between 1 and 13 wt% (see Table S1) to moderate the surface interactions.

All mixtures showed shear thinning behaviour, as seen in Figure 5A. Not surprisingly, the shear thinning behaviour of WPM-containing systems was greater than that of the equivalent dispersions with D[5], due to the more shear thinning nature

of WPM alone. A second plateau at the $\dot{\gamma} = 2000$ s^{-1} was observed for almost all the mixtures, with only WPM + W[8] showing a statistical deviation of over 5% between the last two consecutive data points (Figure 5A). The inset of Figure 5A shows the measurements between $\dot{\gamma}$ = 500 and 2000 s^{-1} for mixtures of W with D[5] or WPM. Within this range of $\dot{\gamma}$ and at a constant [W] (in free water), the shear thinning behaviour of the mixtures was similar, giving rise to almost the same η_{2000} for each of the pairs D[5] + W[1] and WPM + W[1]; D[5] + W[5] and WPM + W[3]; D[5] + W[11] and WPM + W[8] (Figure 5A). Thus the viscous lubrication behaviour for each of the above mentioned pairs in the EHL or hydrodynamic lubrication (*HL*) regimes was expected to be similar (see Figure 4).

At $u \sim 0.001$ m s^{-1}, the μ of D[5] + W[11] and WPM + W[8] did not level off and therefore, the boundary μ cannot be derived from the MTM2 measurements (Figure 5B). The μ of D[5] + W[5] at the lowest u approached to that of W[5] (Figures 3A and 4B). For D[5] + W[1] and WPM + W[1], the onset of the boundary regime can be discerned, signalling a lower boundary μ for WPM + W[1] (Figure 5B) which originates from the greater proportion of surface active moieties when both W and WPM are present and also the potential interposition of W between the microgel particles (Figure 4). The μ curve for D[5] + W[1] (Figure 5B) suggested that the boundary μ would eventually settle at values higher than for W[5], anticipated by the concentration-dependant friction reduction behaviour of W observed elsewhere (Zembyla, 2021).

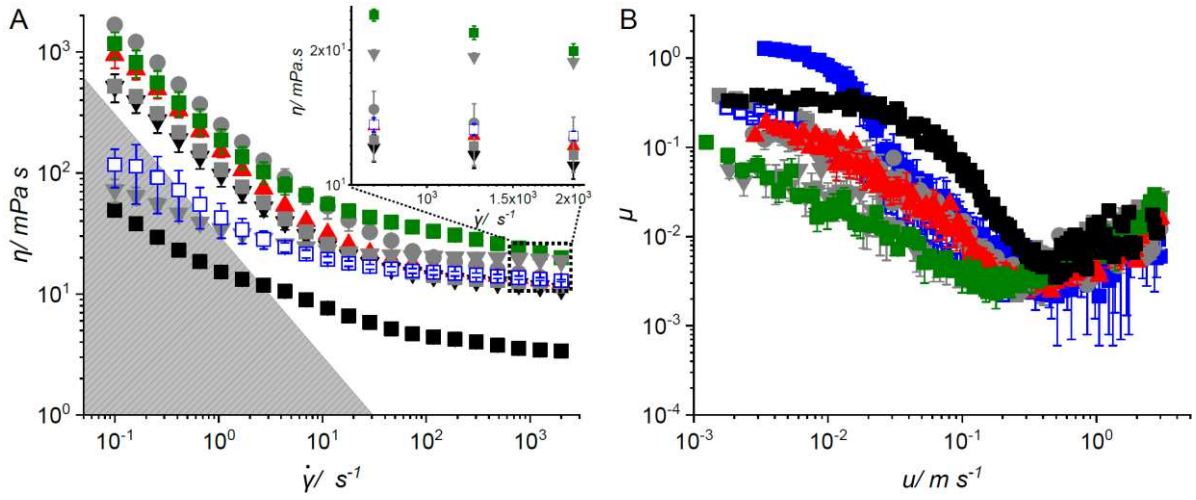

743

744 **Figure 5.** Comparison of (A) flow curves and (B) friction coefficient results for: microgel
745 + whey protein mixtures WPM + W[1] (●), WPM + W[3] (▲), WPM + W[8] (■) against
746 dextran + whey protein mixtures D[5] + W[1] (■), D[5] + W[5] (□), and D[5] + W[11]
747 (▼). The inset in A shows a zoomed in view for shear rates between 500 and 2000 s^{-1}.
748 Note the whey protein concentration in free water (i.e., water content excluding WPM
749 or D) was the same for each of the pairs D[5] + W[1] and WPM + W[1]; D[5] + W[5]
750 and WPM + W[3]; D[5] + W[11] and WPM + W[8]. (For more information see Table
751 S1).

752

753 An interesting finding was observed in the mixed lubrication regime where the
754 $\mu - u$ curves overlapped for each of the afore-mentioned pairs (Figure 5B). This
755 observation has two important implications, which are as follows:

756 (i) The colloidal dispersions of WPM particles behave as a Newtonian fluid
757 within the tribologically-relevant $\dot{\gamma}$ values in the mixed regime and conditions defined
758 in this work. Using eq. (5), h_c values were calculated for WPM dispersion in W
759 solutions at u values reflecting the mixed regime just before its transition to the
760 boundary regime. These values were set at 0.015 and 0.01 m s^{-1} for WPM + W[1] and

761 WPM + W[3], respectively. A value of 0.002 m s^{-1} was assumed for WPM + W[8], since
762 the transition to the boundary was not evident (Figure 5B). The corresponding h_c
763 values were 0.437, 0.330 and 0.163 μm in order of increasing [W], which are 1.5 -
764 3.8× higher than the size of the WPM. Thus at $h_c/d_h > \sim 2$ and these correspondingly
765 high shear rates ($\dot{\gamma}$ > 10^4 s^{-1}) the WPM dispersions showed Newtonian behaviour in
766 the mixed regime. A more detailed study is required to assess the critical h_c/d_h ratio,
767 the rheological parameters and microgel properties at which the microgel particles
768 behave in Newtonian manner, particularly when the hydrodynamic forces are not
769 sufficient to fully separate contact bodies.
770
771 (ii) By optimising a combination of WPM and (non-microgelled) W, combined
772 viscous and thin-film lubricity could be achieved through a single-component, i.e.,
773 whey protein, without the need of any polysaccharide. In this way, proteinaceous
774 lubricants could be developed with no need for including a lipid or polysaccharide
775 component but still meeting the satiety requirements.
776
777 In order to further elucidate the mechanism of action of WPM in its mixtures
778 with W, we plotted the μ curves in Figure 5B as a function of reduced speed
779 parameter, $\eta_{2000} \times u$, (de Vicente, 2005; Sarkar, 2021) as shown in Figure 6. For
780 Newtonian fluids with no apparent surface interactions (*e.g.* adsorption or bonding) or
781 viscous-driven surface separation effects, the shear stresses at the contact surfaces
782 are expected to be independent of the lubricant η and the $\mu - \eta_{2000} \times u$ curves are
783 expected to collapse into a single '*master*' curve, shown as the solid grey line in Figure
784 6.
785

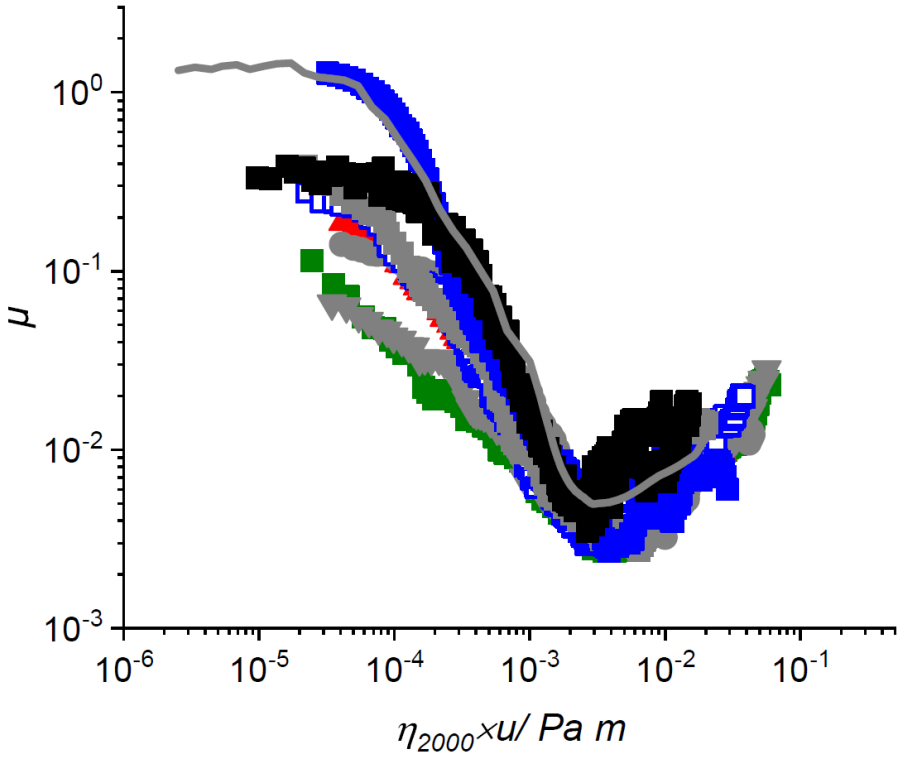

786

787 **Figure 6.** Friction curves normalised to the viscosity at a shear rate of 2000 s^{-1} for
788 microgel and whey protein mixtures WPM + W[1] (●), WPM + W[3] (▲), WPM + W[8]
789 (■) and also for dextran + whey protein mixtures D[5] + W[1] (■), D[5] + W[5] (□),
790 and D[5] + W[11] (▼). The solid-grey line is the curve for a Newtonian fluid (see text).
791 For clarity, the error bars are excluded from graphs.

792

793 Figure 6 shows a similar *EHL* or *HL* μ value for each of the compared pairs. Also, u_{EHL}
794 was similar for the Newtonian fluid and mixtures of D + W or WPM + W, in agreement
795 with the observations of Andablo-Reyes, et al. (Andablo-Reyes, 2019). This work
796 demonstrated that the lubrication performance of colloidal WPM dispersions in the
797 *EHL* and *HL* regimes can be approximated as Newtonian fluids (Andablo-Reyes,
798 2019). This originates from the fact that the predominant source of friction in the *HL*
799 regime is the viscous drag within the lubricant (Andablo-Reyes, 2019; Sarkar, 2021).

Upon addition of WPM or D[5] to W[1] solutions, the absolute value of the characteristic tangent to the $\mu - \eta_{2000} \times u$ curve in mixed regime decreased (Figure 6) with an increase in η_{2000} (see Figure 5A). Further increase in [W] (*i.e.* WPM + W[3] and D[5] + W[5]) did not show a noticeable influence on the mixed μ (Figure 6) or on the η_{2000} results (Figure 5A). The most distinct decrease in the mixed μ was observed at the highest [W] (*i.e.* WPM + W[8] and D[5] + W[11]), coinciding with the largest increase in the η_{2000}. These observations concur with those of Selway et al. (Selway, 2017) and corroborate our findings presented in the previous section: the viscous forces impede fluid squeeze-out and de-wetting of the contacts at the asperity level and therefore reduce the collision frequency between asperities.

3.3.3 Soft tribology using tongue-mimicked surfaces

Due to the lengthy procedures in preparing and cleaning the soft tribology surfaces, not all the above combinations of W, D and WPM were tested with these surfaces. Rather we focussed on those systems that showed the most interesting and unexpected behaviour as evidenced by the MTM2 measurements to provide insights into their lubricity when surface topography, elasticity and wettability emulate the papillae and tribologically relevant features of real human tongue surfaces.

The μ results for HEPES buffer, W[5], D[11], D[5] + W[5], D[11] + W[5], D[5] + W[11] and also microgel systems (WPM, WPM + D[11] and Conj(D[11] + W[5])MG) are shown in Figure 7A. Fluctuations in the μ are probably due to the roughness of the deformable elastomer (*i.e.* filiform and fungiform-papillae) and flat-on-flat tribo-testing geometry. Except for solutions with [D] = 11 wt% and the conjugate microgel, the μ remained almost constant at 0.2 – 0.3 at $5 \times 10^{-5} < u < 10^{-2}$ m s^{-1}, 60% lower than for the buffer.

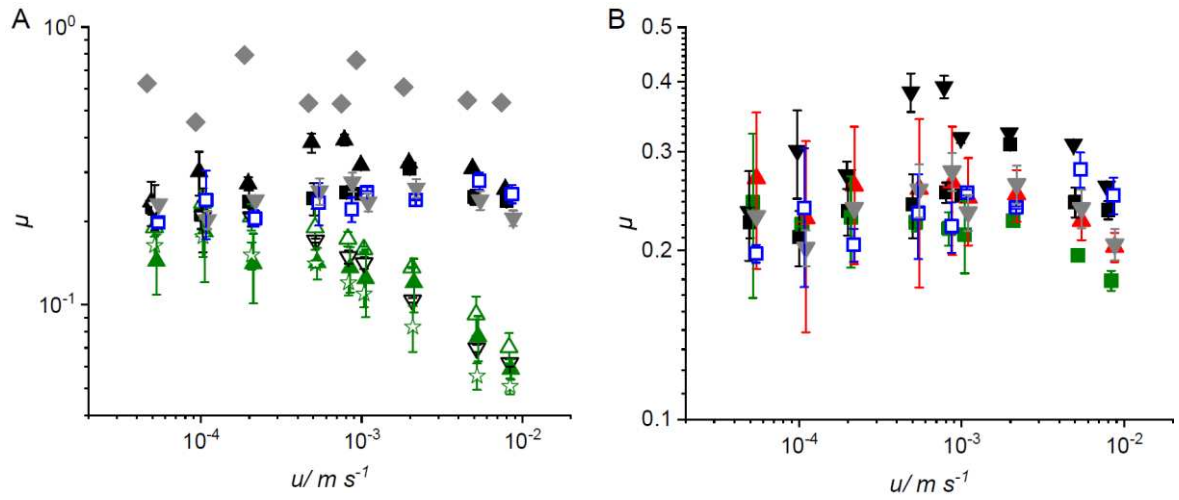

825

826 **Figure 7.** (A) Friction coefficient (μ) *versus* entrainment speed (u) measured using 3D
827 tongue-mimicking surfaces for: buffer (♦), W[5] (■), D[11] (▲), D[5] + W[5] (□), D[11]
828 + W[5] (△),D[5] + W[11] (▼) and also microgel systems WPM (▼), WPM + D[11] (▽)
829 and Conj(D[11] + W[5])MG (★). (B) Comparison of μ *versus* u for D[5] + W[5] (□), D[5]
830 + W[11] (▼), WPM + W[3] (▲) and WPM + W[8] (■). Means are calculated based on
831 readings on at least triplicate samples (n ≥ 3). Note the fluctuations in the μ are
832 probably due to the filiform and fungiform-papillae induced roughness of the
833 deformable elastomer used and flat-on-flat tribo-testing geometry.

834 The flat-on-flat testing configuration lacks the converging contact wedge at the
835 contact inlet (found in ball-on-disc contacts) which mainly supports the build-up of fluid
836 pressurisation and hydrodynamic lift forces to form a lubricant film (see Figure 4).
837 Therefore, the speed-dependant pressurisation of the fluid trapped between the
838 papillae is not expected to contribute to lubricity except through the '*boosted*'
839 mechanism (Walker, Dowson, Longfield, & Wright, 1968). This is particularly valid
840 considering the high permeability of the fluid through the gaps between papillae (de
841 Boer, et al., 2020). Therefore, the origin of friction in this configuration is a sum of
842 shear stresses experienced by individual papillae, particularly fungiform-mimicked

843 domes, which will be more likely to be in contact with the counter body (*i.e.* the steel
844 plate). The monotonic μ behaviour of WPM, W[5] and D[5] + W[5] and D[5] + W[11]
845 dispersions (Figure 7A) implies solid-solid contacts between the bodies with the lower
846 μ values (compared to that of the buffer) indicating a '*thin-film hydration'* mechanism
847 offered by the hydrophilic dispersed phase (*i.e.* WPM, W and D) (Andablo-Reyes,
848 2020; Klein, 2013; Sarkar, 2021).

849 The dispersions with [D] = 11% and Conj(D[11] + W[5])MG) showed similar μ
850 values to other dispersions at $5 \times 10^{-5} < u < 10^{-4}$ m s^{-1}, suggesting a boundary
851 regime (Figure 7A). This was followed by a linear drop in μ values as a function of
852 increasing speed, reaching values between 0.05 and 0.07. The dome-shaped nature
853 of mimicked-fungiform probably provides a converging contact inlet and therefore
854 promotes hydrodynamic forces upon increase in sliding speed, which scale up with
855 increased η values. Therefore, at higher speeds (with the high viscosity fluids, 0.037
856 to 0.124 Pa) the fluid was probably forced into the contact zone, bringing about a drop
857 in μ and transition into the mixed regime.

858 The other noteworthy observation is the overlapping boundary μ of D[11] with
859 those of W[5] or WPM-containing dispersions (Figure 7A), in contrast to the MTM2
860 results (Figures 3A and 3B). This might be attributed to enhanced wettability of the
861 contact surfaces in the tongue-mimicked system decaying dynamic lubricant de-
862 wetting and extending the micro-EHL into the boundary regime (Dowson, 1995), since
863 the squeeze-out dynamics will be hampered by the stronger spread of the lubricant.
864 An additional observation is that Conj(D[11] + W[5])MG) showed no outstanding
865 benefit (Figure 7A), unlike the superlubricous behaviour that this system showed in
866 the MTM2 measurements. This might be due to the absence of: (i) the rolling contact
867 (*i.e.* 3D tongue-mimicking setup operates under pure sliding) which is of paramount

868 importance in entrainment of particles into the contact interface (Yakubov, 2015); or
869 (ii) *cushioning* effect in the tongue-mimic surfaces. Using eq. 5, the calculated h_c and
870 h_{min} at $u = 10^{-4}$ m s^{-1} - the speed just before transition to the mixed regime - were
871 0.067 and 0.029 μm, respectively. These contact gap dimensions are at least three
872 times smaller than the d_H of the Conj(D[11] + W[5])MG) particles (see Table 2). As
873 shown schematically in Figure 4, this would clearly prevent the cushioning effect and
874 particle entrainment especially in the absence of rolling contacts.
875 There are notable differences between the tribotests with the MTM2 and the
876 tongue-mimic setup, including their contact configuration and materials. Soft oral
877 tribology examinations using MTM2 have been often performed under combined
878 rolling-sliding contacts which incorporate rolling friction, a factor absent in the 3D-
879 mimicked setup. The contribution of rolling friction in mouth is still ambiguous and
880 needs more attention. In the MTM2, the large compliant contact area (15.2 mm^2)
881 compared to that of the tongue-mimicked setup (0.3 mm^2), as estimated by Hertzian
882 contact theory, dominates lubricant entrainment and escalates any particle exclusion
883 or confinement effects, whilst the tongue-mimicked setup is a much more realistic
884 representation of tribo-contacts in the mouth, where particle confinement is only likely
885 to occur locally, around papillae features. Furthermore, the large compliant contact
886 area in the MTM2 is likely to accelerate fluid-film squeeze-out (Lorenz, 2013), whilst
887 the textured topography of the tongue mimic (and the tongue) can provide a sustained
888 reservoir of lubricant feeding the contact interface (*i.e. boosted* lubrication) (Walker,
889 1968). Surface patterning has recently gained significant interest in tribology as a way
890 of providing improved lubricity and load-carrying capacity of lubricant films (Gachot,
891 Rosenkranz, Hsu, & Costa, 2017; He, Chen, & Jane Wang, 2008; Murarash, Itovich,

892 & Varenberg, 2011). Nature has probably selected the optimized tongue topography
893 to deliver just the right lubricity and perception simultaneously.

894 In order to verify that WPM provides the same thickening effect as D[5] but also
895 thin-film lubricity, mixtures of WPM or D[5] with W were also investigated on the tongue
896 mimic setup. The results are shown in Figure 7B and it is seen that μ of all the mixtures
897 remained the same at 0.2 to 0.3 until the $u \sim 5 \times 10^{-3}$ m s^{-1}. The higher bulk viscosity
898 mixtures (i.e., D[5] + W[11] and WPM + W[8]) appeared to exhibit a transition between
899 boundary and mixed lubrication regimes manifested in a slight drop in the μ at $u >$
900 5×10^{-3} m/s, again due to a slower lubricant squeeze-out. The slightly improved
901 boundary lubricity of mixtures of WPM + W as compared to D[5] + W (MTM2 results,
902 Figure 5B), was not obvious with the tongue-mimicked setup probably due to the
903 aforementioned differences. Apart from this, the results in Figure 7B corroborate the
904 findings with the MTM2 and confirm that proteinaceous microgels can deliver the same
905 desirable effect of polysaccharides. Thus, intelligently combining proteinaceous
906 microgels plus free (non-microgelled) protein may be able to satisfy both the viscous
907 and thin-film lubricity required and food design requirements, whilst aiding clean label
908 designation.

Conclusions

This study examined the oral-tribological and flow behaviour of Newtonian D solutions when combined with W and their corresponding microgels. PDMS ball on disk friction measurements demonstrated the ability of D and W to provide *viscous* and *thin-film* lubricity, respectively, and the contribution of viscosity-induced enhanced *dynamic-wetting* of surfaces, hence lower friction coefficients, only when they were mixed. W microgels (WPM) imparted *thin-film* lubricity, probably through a *rolling* mechanism, and *viscous* lubricity to almost the same extent as obtained with W[5] and D[5], respectively. Combined WPM + D systems showed a similar enhanced *dynamic-wetting* with boosted *viscous lubricity*, due to the enhanced bulk viscosity of these mixtures. Microgels formed from the W-D conjugate, Conj(D[11] + W[5])MG , showed superlubricity behaviour in the ball-on-disk measurements, where the lubricant film thickness was estimated to be of the order of the hydrodynamic size of the microgel particles. We hypothesized that this may be due to a *cushioning lubrication* mechanism where the contact bodies are fully separated by a closely-packed layer of microgels. However, the superlubricity of Conj(D[11] + W[5])MG was not evident in friction measurements with a tongue mimic surface mounted onto the top surface of a cone and plate rheometer type apparatus (against stainless steel as the lower plate). This was attributed to much lower calculated surface contact separations and a lack of rolling contacts in the tongue-mimic setup. Measurements with both types of tribometer showed that combinations of W and WPM should be able to provide desirable oral lubricity and mouth feel without resorting to combinations of polysaccharide additives and fat/oil dispersions. This would bring about a new perspective for food manufacturers in terms of reformulation by minimizing the number of additives used, without compromising any pleasurable mouth-feel.

Acknowledgement

This study was funded by the European Research Council (ERC) under the European Un-ion's Horizon 2020 research and innovation programme (Grant agreement n° 757993 and 890644) and was carried out at the University of Leeds.

References

Andablo-Reyes, E., Bryant, M., Neville, A., Hyde, P., Sarkar, R., Francis, M., & Sarkar, A. (2020). 3D biomimetic tongue-emulating surfaces for tribological applications. *ACS Applied Materials & Interfaces, 12*(44), 49371-49385.

Andablo-Reyes, E., Yerani, D., Fu, M., Liamas, E., Connell, S., Torres, O., & Sarkar, A. (2019). Microgels as viscosity modifiers influence lubrication performance of continuum. *Soft Matter, 15*(47), 9614-9624.

Araiza-Calahorra, A., Glover, Z. J., Akhtar, M., & Sarkar, A. (2020). Conjugate microgel-stabilized Pickering emulsions: Role in delaying gastric digestion. *Food Hydrocolloids, 105*, 105794.

Carrasco, F., Chornet, E., Overend, R. P., & Costa, J. (1989). A generalized correlation for the viscosity of dextrans in aqueous solutions as a function of temperature, concentration, and molecular weight at low shear rates. *37*(8), 2087-2098.

Cassin, G., Heinrich, E., & Spikes, H. A. (2001). The influence of surface roughness on the lubrication properties of adsorbing and non-adsorbing biopolymers. *Tribology Letters, 11*(2), 95-102.

de Boer, G. N., Raske, N., Soltanahmadi, S., Dowson, D., Bryant, M. G., & Hewson, R. W. (2020). A porohyperelastic lubrication model for articular cartilage in the natural synovial joint. *Tribology International, 149*, 105760.

de Vicente, J., Stokes, J. R., & Spikes, H. A. (2005). The frictional properties of Newtonian fluids in rolling–sliding soft-EHL contact. *Tribology Letters, 20*(3), 273-286.

Dissanayake, M., Ramchandran, L., & Vasiljevic, T. (2013). Influence of pH and protein concentration on rheological properties of whey protein dispersions. *International Food Research Journal, 20*(5), 2167.

Dowson, D. (1995). Elastohydrodynamic and micro-elastohydrodynamic lubrication. *Wear, 190*(2), 125-138.

Gachot, C., Rosenkranz, A., Hsu, S. M., & Costa, H. L. (2017). A critical assessment of surface texturing for friction and wear improvement. *Wear, 372-373*, 21-41.

Goren, T., Spencer, N., & Crockett, R. J. R. A. (2014). Impact of chain morphology on the lubricity of surface-grafted polysaccharides. *4*(41), 21497-21503.

Griesser, H. J., Hartley, P. G., McArthur, S. L., McLean, K. M., Meagher, L., & Thissen, H. (2002). Interfacial properties and protein resistance of nano-scale polysaccharide coatings. *Smart Materials and Structures, 11*(5), 652-661.

Hamrock, B. J., & Dowson, D. (1978). Elastohydrodynamic lubrication of elliptical contacts for materials of low elastic modulus I—fully flooded conjunction. *Journal of Lubrication Technology, 100*(2), 236-245.

He, B., Chen, W., & Jane Wang, Q. (2008). Surface texture effect on friction of a microtextured poly(dimethylsiloxane) (PDMS). *Tribology Letters, 31*(3), 187.

Hu, J., Andablo-Reyes, E., Soltanahmadi, S., & Sarkar, A. (2020). Synergistic microgel-reinforced hydrogels as high-performance lubricants. *ACS Macro Letters, 9*(12), 1726-1731.

Käsdorf, B. T., Weber, F., Petrou, G., Srivastava, V., Crouzier, T., & Lieleg, O. (2017). Mucin-inspired lubrication on hydrophobic surfaces. *Biomacromolecules, 18*(8), 2454-2462.

Kew, B., Holmes, M., Stieger, M., & Sarkar, A. (2021). Oral tribology, adsorption and rheology of alternative food proteins. *Food Hydrocolloids, 116*, 106636.

Klein, J. (2013). Hydration lubrication. *Friction, 1*(1), 1-23.

Lee, S., Iten, R., Müller, M., & Spencer, N. D. (2004). Influence of molecular architecture on the adsorption of poly(ethylene oxide)−poly(propylene oxide)−poly(ethylene oxide) on PDMS surfaces and implications for aqueous lubrication. *Macromolecules, 37*(22), 8349-8356.

Liu, K., Tian, Y., Stieger, M., van der Linden, E., & van de Velde, F. (2016). Evidence for ball-bearing mechanism of microparticulated whey protein as fat replacer in liquid and semi-solid multi-component model foods. *Food Hydrocolloids, 52*, 403-414.

Lorenz, B., Krick, B. A., Rodriguez, N., Sawyer, W. G., Mangiagalli, P., & Persson, B. N. J. (2013). Static or breakloose friction for lubricated contacts: the role of surface roughness and dewetting. *Journal of Physics: Condensed Matter, 25*(44), 445013.

Martwiset, S., Koh, A. E., & Chen, W. (2006). Nonfouling characteristics of dextran-containing surfaces. *Langmuir, 22*(19), 8192-8196.

McLean, K. M., Johnson, G., Chatelier, R. C., Beumer, G. J., Steele, J. G., & Griesser, H. J. (2000). Method of immobilization of carboxymethyl-dextran affects resistance to tissue and cell colonization. *Colloids and Surfaces B: Biointerfaces, 18*(3), 221-234.

Murarash, B., Itovich, Y., & Varenberg, M. (2011). Tuning elastomer friction by hexagonal surface patterning. *Soft Matter, 7*(12), 5553-5557.

Myant, C., Fowell, M., Spikes, H. A., & Stokes, J. R. (2010). An investigation of lubricant film thickness in sliding compliant contacts. *Tribology Transactions, 53*(5), 684-694.

Oliver, C. M., Melton, L. D., & Stanley, R. A. (2006). Creating proteins with novel functionality via the Maillard reaction: A review. *Critical Reviews in Food Science and Nutrition, 46*(4), 337-350.

Österberg, E., Bergström, K., Holmberg, K., Schuman, T. P., Riggs, J. A., Burns, N. L., Van Alstine, J. M., & Harris, J. M. (1995). Protein-rejecting ability of surface-bound dextran in end-on and side-on configurations: Comparison to PEG. *29*(6), 741-747.

Perrino, C., Lee, S., Choi, S. W., Maruyama, A., & Spencer, N. D. (2008). A biomimetic alternative to poly(ethylene glycol) as an antifouling coating: resistance to nonspecific protein adsorption of poly(l-lysine)-graft-dextran. *Langmuir, 24*(16), 8850-8856.

1023 Perrino, C., Lee, S., & Spencer, N. D. (2009). End-grafted sugar chains as aqueous
1024 lubricant additives: synthesis and macrotribological tests of poly(l-lysine)-graft-
1025 dextran (PLL-g-dex) copolymers. *Tribology Letters, 33*(2), 83-96.
1026 Persson, B. N. (2006). Rubber friction: role of the flash temperature. *Journal of*
1027 *Physics: Condensed Matter, 18*(32), 7789.
1028 Piehler, J., Brecht, A., Hehl, K., & Gauglitz, G. (1999). Protein interactions in covalently
1029 attached dextran layers. *Colloids and Surfaces B: Biointerfaces, 13*(6), 325-
1030 336.
1031 Pradal, C., & Stokes, J. R. (2016). Oral tribology: bridging the gap between physical
1032 measurements and sensory experience. *Current Opinion in Food Science, 9*,
1033 34-41.
1034 Rao, M. A. (2014). Flow and functional models for rheological properties of fluid foods.
1035 In *Rheology of Fluid, Semisolid, and Solid Foods: Principles and Applications*
1036 (pp. 27-61). Boston, MA: Springer US.
1037 Reddyhoff, T., Schmidt, A., & Spikes, H. (2019). Thermal conductivity and flash
1038 temperature. *Tribology Letters, 67*(1), 22.
1039 Rosenberg, K. J., Goren, T., Crockett, R., & Spencer, N. D. (2011). Load-induced
1040 transitions in the lubricity of adsorbed poly(l-lysine)-g-dextran as a function of
1041 polysaccharide chain density. *ACS Applied Materials & Interfaces, 3*(8), 3020-
1042 3025.
1043 Sarkar, A., Andablo-Reyes, E., Bryant, M., Dowson, D., & Neville, A. (2019).
1044 Lubrication of soft oral surfaces. *Current Opinion in Colloid & Interface Science,*
1045 *39*, 61-75.
1046 Sarkar, A., Kanti, F., Gulotta, A., Murray, B. S., & Zhang, S. (2017). Aqueous
1047 lubrication, structure and rheological properties of whey protein microgel
1048 particles. *Langmuir, 33*(51), 14699-14708.
1049 Sarkar, A., & Krop, E. M. (2019). Marrying oral tribology to sensory perception: a
1050 systematic review. *Current Opinion in Food Science, 27*, 64-73.
1051 Sarkar, A., Murray, B., Holmes, M., Ettelaie, R., Abdalla, A., & Yang, X. (2016). In vitro
1052 digestion of Pickering emulsions stabilized by soft whey protein microgel
1053 particles: influence of thermal treatment. *Soft Matter, 12*(15), 3558-3569.
1054 Sarkar, A., Soltanahmadi, S., Chen, J., & Stokes, J. R. (2021). Oral tribology: Providing
1055 insight into oral processing of food colloids. *Food Hydrocolloids, 117*, 106635.
1056 Selway, N., Chan, V., & Stokes, J. R. (2017). Influence of fluid viscosity and wetting
1057 on multiscale viscoelastic lubrication in soft tribological contacts. *Soft Matter,*
1058 *13*(8), 1702-1715.
1059 Sills, S., Vorvolakos, K., Chaudhury, M. K., & Overney, R. M. (2007). Molecular origins
1060 of elastomeric friction. In E. Gnecco & E. Meyer (Eds.), *Fundamentals of*
1061 *Friction and Wear* (pp. 659-676). Berlin, Heidelberg: Springer Berlin
1062 Heidelberg.
1063 Stokes, J. R., Boehm, M. W., & Baier, S. K. (2013). Oral processing, texture and
1064 mouthfeel: From rheology to tribology and beyond. *Current Opinion in Colloid*
1065 *& Interface Science, 18*(4), 349-359.
1066 Stokes, J. R., Macakova, L., Chojnicka-Paszun, A., de Kruif, C. G., & de Jongh, H. H.
1067 J. (2011). Lubrication, adsorption, and rheology of aqueous polysaccharide
1068 Solutions. *Langmuir, 27*(7), 3474-3484.
1069 Sun, W.-W., Yu, S.-J., Yang, X.-Q., Wang, J.-M., Zhang, J.-B., Zhang, Y., & Zheng,
1070 E.-L. (2011). Study on the rheological properties of heat-induced whey protein
1071 isolate–dextran conjugate gel. *Food Research International, 44*(10), 3259-
1072 3263.

Sun, W.-W., Yu, S.-J., Zeng, X.-A., Yang, X.-Q., & Jia, X. (2011). Properties of whey protein isolate–dextran conjugate prepared using pulsed electric field. *Food Research International, 44*(4), 1052-1058.

Tirtaatmadja, V., Dunstan, D. E., & Boger, D. V. (2001). Rheology of dextran solutions. *Journal of Non-Newtonian Fluid Mechanics, 97*(2), 295-301.

Vakis, A. I., Yastrebov, V. A., Scheibert, J., Nicola, L., Dini, D., Minfray, C., Almqvist, A., Paggi, M., Lee, S., Limbert, G., Molinari, J. F., Anciaux, G., Aghababaei, R., Echeverri Restrepo, S., Papangelo, A., Cammarata, A., Nicolini, P., Putignano, C., Carbone, G., Stupkiewicz, S., Lengiewicz, J., Costagliola, G., Bosia, F., Guarino, R., Pugno, N. M., Müser, M. H., & Ciavarella, M. (2018). Modeling and simulation in tribology across scales: An overview. *Tribology International, 125*, 169-199.

Walker, P. S., Dowson, D., Longfield, M. D., & Wright, V. (1968). "Boosted lubrication" in synovial joints by fluid entrapment and enrichment. *Annals of the rheumatic diseases, 27*(6), 512-520.

Xu, F., Liamas, E., Bryant, M., Adedeji, A. F., Andablo-Reyes, E., Castronovo, M., Ettelaie, R., Charpentier, T. V. J., & Sarkar, A. (2020). A self-assembled binary protein model explains high-performance salivary lubrication from macro to nanoscale. *Advanced Materials Interfaces, 7*(1), 1901549.

Yakubov, G. E., Branfield, T. E., Bongaerts, J. H. H., & Stokes, J. R. (2015). Tribology of particle suspensions in rolling-sliding soft contacts. *Biotribology, 3*, 1-10.

Yang, X., Li, A., Li, X., Sun, L., & Guo, Y. (2020). An overview of classifications, properties of food polysaccharides and their links to applications in improving food textures. *Trends in Food Science & Technology, 102*, 1-15.

Zembyla, M., Liamas, E., Andablo-Reyes, E., Gu, K., Krop, E. M., Kew, B., & Sarkar, A. (2021). Surface adsorption and lubrication properties of plant and dairy proteins: A comparative study. *Food Hydrocolloids, 111*, 106364.

CRediT author statement

Dr. Siavash Soltanahmadi: Conceptualization, Methodology, Validation, Formal analysis, Investigation, Data curation, Writing- Reviewing & Editing; Visualization; Project administration; Writing- Original draft preparation, Writing- Reviewing & Editing**, Prof. Brent S. Murray:** Conceptualization, Supervision, Writing- Reviewing & Editing; Prof. **Anwesha Sarkar:** Conceptualization, Project administration**;** Writing- Reviewing & Editing, Supervision, Funding acquisition**.**

Conflict of Interests

Declarations of interest: none

Supporting information

Comparison of oral tribological performance of proteinaceous microgel systems with protein-polysaccharide combinations

Siavash Soltanahmadi, Brent S. Murray, Anwesha Sarkar*

Food Colloids and Bioprocessing Group, School of Food Science and Nutrition, University of Leeds, UK

*Corresponding author:

Prof. Anwesha Sarkar

Food Colloids and Processing Group,

School of Food Science and Nutrition, University of Leeds, Leeds LS2 9JT, UK.

E-mail address: A.Sarkar@leeds.ac.uk (A. Sarkar).

Table S1. The composition of the whey protein mixtures with D[5] or WPM.

Sample name	Dextran (wt%)*	Whey protein (wt%)*	Whey protein in free water (wt%)‡	Whey protein microgel (vol%)*
D[5]+ W[1]	5	1	1.06	-
D[5] + W[5]	5	5	5.59	-
D[5] + W[11]	5	11	13.27	-
WPM + W[1]	-	0.62	1.06	41.7
WPM + W[3]	-	3.26	5.59	41.7
WPM + W[8]	-	7.74	13.27	41.7

* The values show the concentrations of the relevant biopolymers (pristine or conjugated) in the total weight/volume of the dispersions.

‡ The values present the concentration of whey protein in free water content (*i.e.* excluding D or WPM and the water trapped in the cross-linked network of WPM) of the mixtures.

Due to the particulate nature of WPM and therefore, for true companions between the influence of D[5] and WPM on flow and lubrication behaviour of their mixtures with whey protein solutions, the concentration of whey protein in free water (i.e. water content excluding WPM or D) was set to be the same for each comparison-pair of D[5] + W[1] and WPM + W[1]; D[5] + W[5] and WPM + W[3]; and D[5] + W[11] and WPM + W[8]. The comparison classes are shaded with the same colour in Table S1.

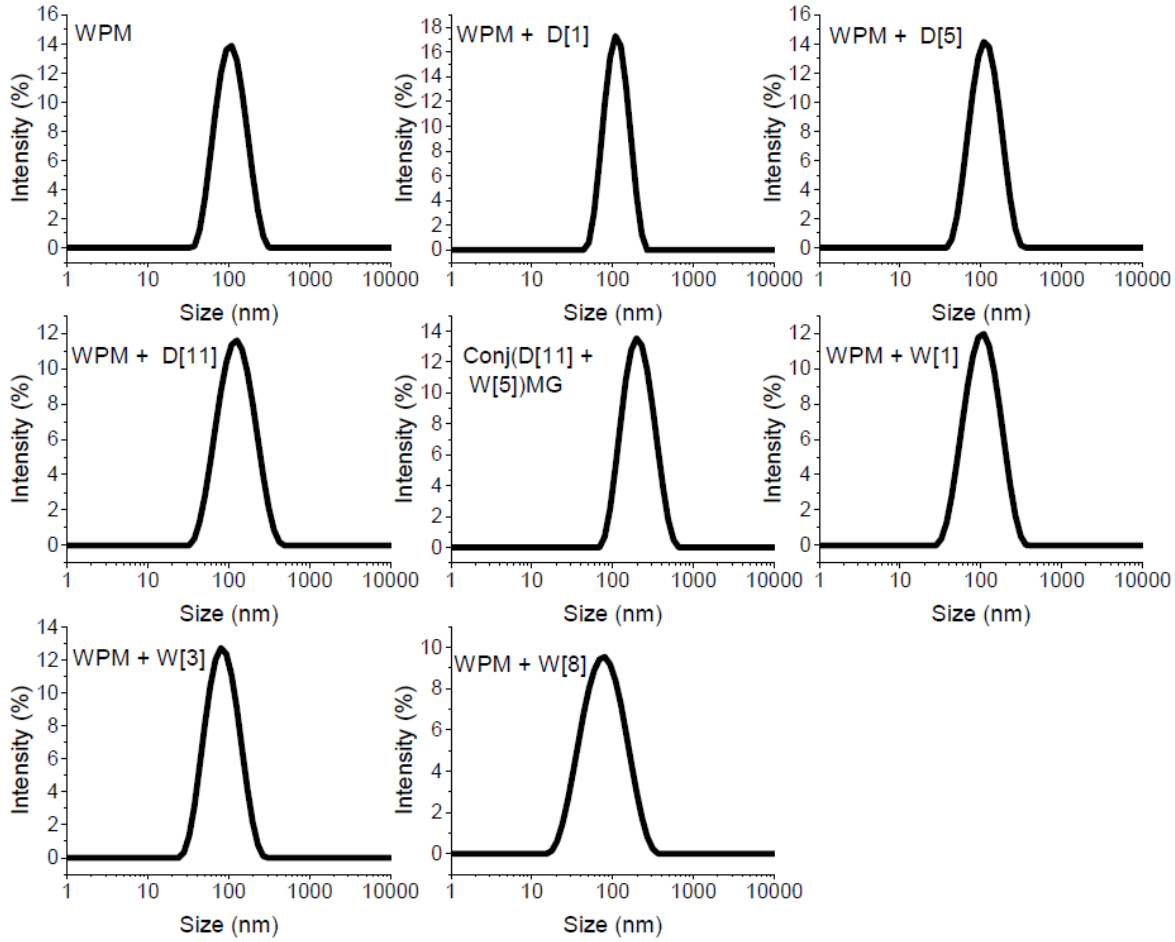

Figure S1. Typical results obtained for size measurements using DLS for microgel systems.

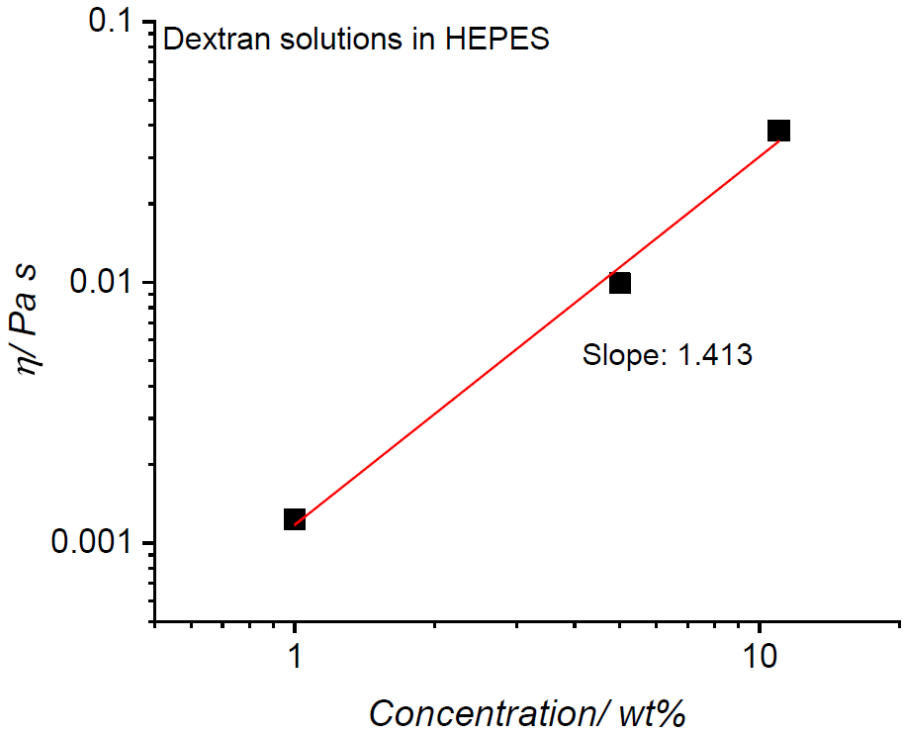

Figure S2. The shear viscosity (η) versus concentration plot in log-log scale for solutions of D[1], D[5] and D[11]. The resultant tangent to the curve obtained by linear fitting showed a slope of 1.4. The same value was reported for dextran with a molecular weight of 2×10^6 by Tirtaatmadja, et al. (Tirtaatmadja, Dunstan, & Boger, 2001). This indicates that the concentrations of dextran used in this study were below the critical concentration where a significant change to the shear viscosity has been observed as a result of an increase in dextran concentration shifting the slope to values of around 4 (Tirtaatmadja, et al., 2001). When below the critical concentration, a compact branched configuration with long side-chain in the branches was suggested for dextran.

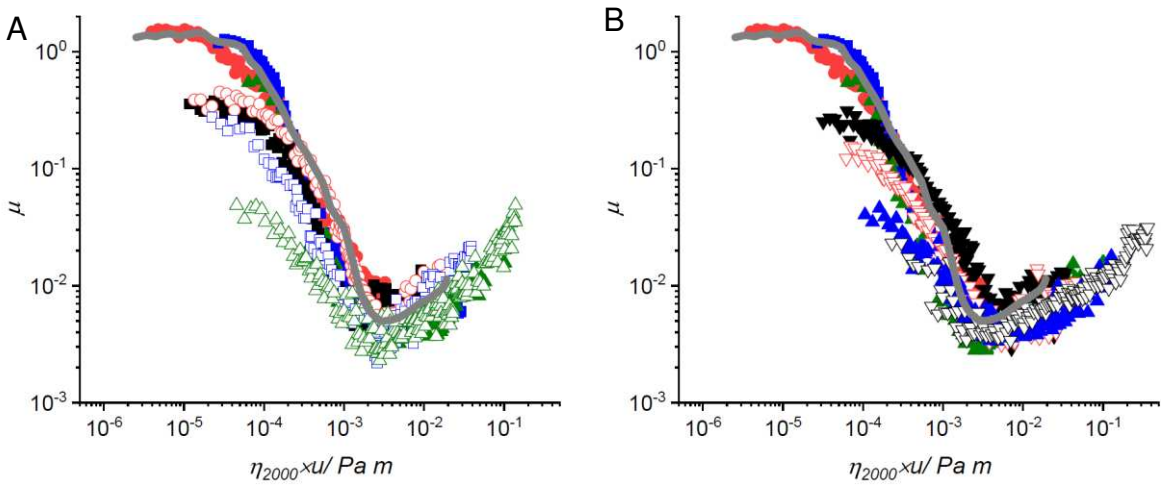

Figure S3. Friction coefficient (μ) *versus* product of the high-shear viscosity (at 2000 s^{-1}) multiplied by the entrainment speed ($\eta_{2000} \times u$) for biopolymer solutions D[1] (●), D[5] (■), D[11] (▲) and W[5] (■) and mixtures of dextran and whey protein D[1] + W[5] (○), D[5] + W[5] (□), D[11] + W[5] (△). (B) μ *versus* $\eta_{2000} \times u$ for biopolymer solutions D[1] (●), D[5] (■), D[11] (▲) and the microgel systems WPM (▼), WPM + D[1] (▽), WPM + D[5] (▲), WPM + D[11]. The '*master*' curve for a typical Newtonian fluid is shown in grey line. Means are calculated based on readings on at least triplicate samples (n ≥ 3). The tests were conducted at 37 °C using MTM 2 on three separate PDMS tribopairs and lubricant samples. Note that the viscosity-shear rate curves for WPM + D[5] and WPM + D[11] did not reach a plateau in the flow measurements and shown for comparison purposes.

References

Tirtaatmadja, V., Dunstan, D. E., & Boger, D. V. (2001). Rheology of dextran solutions. *Journal of Non-Newtonian Fluid Mechanics, 97*(2), 295-301.